UNIVERSITY OF CALIFORNIA SAN DIEGO

Seawater CO_2-Chemistry Variability in the Near-Shore Environment of the Southern California Bight

A Thesis submitted in partial satisfaction of the requirements for the degree

Master of Science

in

Oceanography

by

Samuel Andrew Ho'onewanewaonalani Kekuewa

Committee in charge:

Professor Andreas Andersson, Chair
Professor Andrew Dickson
Professor Todd Martz

2020

The Thesis of Samuel Andrew Ho'onewanewaonalani Kekuewa is approved, and it is acceptable in quality and form for publication on microfilm and electronically:

_____

_____

_____

Chair

University of California San Diego

2020

TABLE OF CONTENTS

LIST OF ABBREVIATIONS

CO_2	Carbon dioxide
DIC	Dissolved inorganic carbon
DO	Dissolved oxygen
OA	Ocean acidification
SD	Standard deviation
TA	Total alkalinity
Ω_{Ar}	Saturation state of seawater with respect to aragonite
IPCC	International Panel on Climate Change
RCP	Representative Concentration Pathway
EBUS	Eastern boundary upwelling system
CCS	California Current System
PFEL	Pacific Fisheries Environmental Laboratory
UI	Upwelling Index
$CaCO_3$	Calcium carbonate
H^+	Hydrogen ion
HCO_3^-	Bicarbonate ion
H_2CO_3	Carbonic acid
CO_3^{2-}	Carbonate ion
SCB	Southern California Bight

LIST OF FIGURES

LIST OF TABLES

ABSTRACT OF THE THESIS

Seawater CO_2-Chemistry Variability in the Near-Shore Environment of the Southern California Bight

by

Samuel Andrew Ho'onewanewaonalani Kekuewa

Master of Science in Oceanography

University of California San Diego, 2020

Professor Andreas Andersson, Chair

Seawater CO_2-chemistry in the Southern California Bight (SCB) has been well characterized at seasonal resolution over the past several decades by multiple research expeditions. However, the near-shore environment (0-2 km) has largely been absent from these surveys and the drivers of seawater CO_2-chemistry variability in this region remain to be fully characterized. In particular, the role of variable upwelling intensity is poorly known, and could have important

implications for near-shore habitats sensitive to low pH and Ω_{Ar} conditions. Here, I present near-shore seawater CO_2-chemistry data based on monthly transects between March 2017 and September 2018 at four stations extending from the Scripps Pier to the 60 m depth contour (~2 km offshore). Seawater samples were analyzed for seawater CO_2-chemistry parameters and were paired with autonomous sensors deployed at 18 m depth. The results showed that during fall and winter, pH and Ω_{Ar} values ranged from 7.9-8.1 and 1.8-2.9 along the transect, respectively. During spring and summer, intensified upwelling transported low pH and Ω_{Ar} seawater to the near-shore region reaching values as low as 7.69 and 0.95, respectively, at depths less than 20 m and within 1 km of the shoreline. The low pH and Ω_{Ar} conditions typically persisted for several months from April to July. The magnitude of change in pH and Ω_{Ar} was correlated with the density of the water, i.e., the higher the density the lower the pH and Ω_{Ar}, but did not show direct correlation with the total amount of water that was upwelled.

Introduction

Since the onset of the Industrial Revolution, the atmospheric carbon dioxide (CO_2) concentration has increased from 280 μmol mol^{-1} in the 1800s (Jansen et al., 2007) to 410 μmol mol^{-1} in 2019 (https://scripps.ucsd.edu/programs/keelingcurve/; Keeling et al., 2001). This increase in CO_2 is primarily the result of fossil fuel combustion, cement production, and land use changes (Friedlingstein et al., 2010; Ciais et al., 2013). However, only 44% of the CO_2 produced from these activities remains in the atmosphere while approximately 29% are absorbed by the terrestrial biosphere and 22% by the oceans (Le Quéré et al., 2018).

As CO_2 dissolves in seawater, some reacts with water to form carbonic acid (H_2CO_3), which dissociates into hydrogen ($[H^+]$), bicarbonate ($[HCO_3^-]$), and carbonate ($[CO_3^{2-}]$) ions (Equation 1). The reaction results in a net increase in hydrogen ions and consequently a decrease in seawater pH (Equation 2). At the same time, $[HCO_3^-]$ increases while $[CO_3^{2-}]$ decreases (Equation 3). The decrease in $[CO_3^{2-}]$ ions results in a decrease in the saturation state of seawater (Ω) with respect to calcium carbonate ($CaCO_3$) minerals, which is defined as the ion concentration (ICP) product of calcium and carbonate ions divided by ICP at equilibrium, i.e., the stoichiometric solubility product (Ksp*) (Equation 4). Ω is unitless and can be viewed as an index of how easy or difficult it is to precipitate or dissolve $CaCO_3$. If Ω > 1, seawater is supersaturated and mineral precipitation is thermodynamically favored, and if Ω < 1, seawater is undersaturated and mineral dissolution is favored. Collectively, the changes occurring in seawater dissolved inorganic carbon chemistry from anthropogenic CO_2 emissions have been referred to as ocean acidification (OA) (Revelle and Suess, 1957; Caldeira and Wickett, 2003; Feely et al., 2008).

$$CO_2(gas) \rightarrow CO_2(aqueous) + H_2O \rightarrow H_2CO_3 \rightarrow HCO_3^- + H^+ \rightarrow CO_3^{2-} + 2H^+ \quad (1)$$

$$pH = -\log(H^+) \quad (2)$$

$$CO_2 + CO_3^{2-} + H_2O \rightarrow 2HCO_3^- \quad (3)$$

$$\Omega = \frac{[Ca^{2+}][CO_3^{2-}]}{K_{sp}} \quad (4)$$

As a result of ocean uptake of anthropogenic CO_2, in recent decades open-ocean pH has on average decreased by 0.0013 to 0.0025 yr^{-1} depending on location (Sabine et al., 2004; Bates and Peters, 2007; Olafsson et al., 2009; Bates et al., 2014). Following the International Panel on Climate Change (IPCC) intermediate Representative Concentration Pathway (RCP) 4.5 scenario, atmospheric CO_2 levels are projected to increase to approximately 530 μmol mol^{-1} by the year 2100. In this emissions scenario, open-ocean seawater pH would decrease by 0.15 pH units from the modern-day typical value of 8.11 to 7.96 by the year 2100 (IPCC, 2014; Feely et al., 2004; Bates et al., 2010). However, if global CO_2-emissions essentially continue unabated (i.e., RCP 8.5), atmospheric CO_2 levels would reach 800 μmol mol^{-1} with an associated decrease in open-ocean seawater pH by 0.3-0.4 units (IPCC, 2014). These scenarios primarily apply to open-ocean environments and rely on basic chemical principles where the primary driver of the secular seawater CO_2 increase is gas exchange at the ocean-atmosphere interface (Feely et al., 2009; Lauvset and Gruber, 2014). Increases in surface seawater pCO_2 in the open ocean generally track atmospheric pCO_2 closely (Bates et al., 2014). As a result, projections of open ocean surface seawater acidification are relatively straightforward (Duarte et al., 2013; Bates et al., 2012).

In contrast to the open ocean, coastal marine systems experience much greater variability in chemical parameters over daily and seasonal timescales resulting in localized surface seawater pCO_2 values that may be radically different from atmospheric pCO_2 (Hoffman et al., 2011; Andersson and Mackenzie, 2012). These environments experience greater variability than the open ocean due to a greater biomass to water volume ratio and productivity, but also due to influence from terrestrial runoff, river and groundwater input, upwelling, tidal flow, and local bathymetry

(Wootton et al., 2008; Frieder et al., 2012; Alin et al., 2012; Hauri et al., 2013; Feely et al., 2016). Overall, these processes produce large spatiotemporal variability in biogeochemical parameters that may mask changes in seawater chemistry owing to increasing atmospheric CO_2 (Cai et al., 2011; Fassbender et al., 2011; Duarte et al., 2013; Andersson et al., 2015). In addition, these processes with a large influence on seawater pH could either exacerbate or alleviate changes in seawater CO_2 chemistry, and thus, the susceptibility of marine ecosystems to OA (Feely et al., 2008; Duarte et al., 2013; Andersson et al., 2014). However, there are currently limited observations of carbon chemistry in coastal environments across both temporal and spatial scales making it challenging to accurately predict future conditions (Andersson et al., 2015). Similarly, to this date, an anthropogenic carbon signal owing to rising atmospheric CO_2 has not unequivocally been recorded in any near shore marine environment as the likely time of emergence exceeds the current duration of observations (Sutton et al., 2019). Nonetheless, temporal declines in seawater pH that exceed those of the open ocean have been reported for some systems including coral reefs (Cyronak et al., 2014) and upwelling systems (Wooton et al., 2008), but have typically been attributed to the influence of processes other than rising atmospheric CO_2 (Wooton et al., 2008; Cyronak et al., 2014)

Eastern boundary upwelling systems (EBUS) have been suggested to be specifically vulnerable to OA due to the complex combination of mixing, tidal signals, and biological activity (Feely et al., 2008; Thomsen et al., 2010; Hoffman et al., 2011; Yu et al., 2011; Gaylord et al., 2011; Gruber et al., 2012; Fenberg et al., 2015). EBUSs already experience large ranges of seawater pH and Ω_{Ar} variability outside the "natural envelope" projected for the open ocean by the end of the century by multiple IPCC RCP scenarios (i.e., 4.5, 6.0, 8.5) (IPCC, 2014; Gruber et al., 2012). In these systems, seasonal variability in the prevailing wind speed and direction results in

upwelling of deep, nutrient-rich waters with low oxygen and low pH into the coastal region (Feely et al., 2008; Chavez et al., 2017). Additionally, EBUSs are some of the most biologically productive areas in the ocean (Pauly and Christensen, 1995), supporting some of the most important and largest fisheries worldwide (Bakun et al., 2015). The high productivity in these systems is driven by the input of remineralized nutrients from the upwelled deep water (Hauri et al., 2009). It has also been proposed that EBUSs may act as either a seasonal source or sink of anthropogenic carbon with respect to the atmosphere depending on ocean basin and the depth of the oxygen minimum zone (Laruelle et al., 2010; Borges et al., 2010; Brady et al., 2019). However, globally, coastal margins may play an important role in sequestering atmospheric CO_2 to the ocean (Hales et al., 2005; Borges et al., 2005) and are estimated to remove 0.19 Pg C yr^{-1} from the atmosphere (Laruelle et al., 2014).

As the oceans continue to absorb a significant proportion of CO_2 produced by human activities, upwelling of low pH and high CO_2 seawater in EBUSs will carry an additional anthropogenic carbon signature, exacerbating the already low pH and high CO_2 conditions in such regions (Gruber et al., 2002; Feely et al., 2008). Concurrently, upwelling is predicted to increase in duration and intensity owing to changing wind patterns arising from climate change (Bograd et al., 2009; Iles et al., 2012; Sydeman et al., 2014; Wang et al., 2015). This will result in longer and intensified exposure of low pH conditions in coastal marine systems (Iles et al., 2012; Wang et al., 2015), which will coincide with shoaling of undersaturated ($\Omega_{Ar} < 1$) and low pH seawater (Feely et al., 2004; Orr et al., 2005; Hauri et al., 2013; Leinweber et al., 2013). A longer exposure to low pH and Ω_{Ar} conditions can have negative effects on both calcifying and non-calcifying marine organisms in these highly productive EBUSs (Orr et al., 2005; Doney et al., 2009; Koch et al., 2013; Gattuso et al., 2015).

The California Current System (CCS) is an example of an EBUS that has received substantial attention for the past several decades through seasonally repeated ship surveys including the California Cooperative Oceanic Fisheries Investigations (CalCOFI) and California Current Ecosystem Long Term Ecological Research (Alin et al., 2012). Beginning in 2008, CalCOFI started the collection of seawater samples to measure dissolved inorganic carbon (DIC) and total alkalinity (TA) in order to determine long-term trends in carbonate chemistry within the CCS (https://calcofi.org/ccdata/dic-data.html). These data are essential to assess the current conditions and the potential vulnerability of marine organisms and ecosystems living within the CCS in the context of OA (Hare et al., 2007). It also provides critical observations that are required to guide future model predictions of seawater CO_2 variability in this system (Cai et al., 2011; Feely et al., 2009; Andersson et al., 2013). However, despite the extensive CalCOFI data, there is a lack of observations and knowledge of the spatiotemporal variability of seawater carbonate chemistry in the proximal near-shore environment (i.e., within 2 km of the shoreline) (Hoffman et al., 2011). This near-shore region is disproportionately important to many marine organisms (i.e., oysters, urchins, lobsters, mussels, and coralline algae) and ecosystems (i.e., kelp forests, rocky intertidal) and therefore warrants further investigation of the CO_2-chemistry in these environments and potential vulnerability of these organisms to OA (Pauly et al., 2002; Yu et al., 2011; Frieder et al., 2013; Silbiger et al., 2019).

Recent advances in the accuracy and resolution of autonomous sensors has led to an increase in studies monitoring high-temporal variability of coastal marine systems (Martz et al., 2010; Hoffman et al., 2011; Friedrich et al., 2012; Leinweber et al., 2012; Takeshita et al., 2015; Kapsenberg et al., 2016), including in the Southern California Bight (SCB). For example, Takeshita et al. (2015) illustrated that distinct near-shore environments (i.e., surf zone, kelp forest,

canyon edge, and shelf break) in the SCB experienced different mean daily ranges in pH (0.085, 0.054, 0.120, 0.053) and Ω_{Ar} (0.46, 0.22, 0.48, 0.14) despite close geographical proximity (< 5 km). Takeshita et al. (2015) did not fully interpret the differences in biogeochemical variability but did attribute some of these differences to variation in depth between sites. The largest diel variability of pH and Ω_{Ar} (0.120 and 0.48) was observed at the canyon edge due to the advection of deep water from a submarine canyon (Navarro et al., 2013). Furthermore, this study highlighted that week to month scale variability was 3 times larger than diel variability in the kelp forest. Takeshita et al. (2015) attributed this difference to changing water masses, stratification, and increased biological respiration that operate on longer timescales. Similar studies in the SCB observed how larger biomasses of macrophytes (ie., kelp and seagrass) alleviated low pH through photosynthesis and hypothesized that these systems may provide temporal refuges for local marine organisms to future OA conditions (Frieder et al., 2012; Kapsenberg et al., 2016). However, both studies acknowledge that this hypothesis is dependent on how other stressors such as temperature, nutrients, and oxygen affect the macrophytes ability to provide a refuge in the future (Frieder et al., 2012; Kapsenberg et al., 2016). Data from these studies and similar studies (Frieder et al., 2012; Takeshita et al., 2015; Kapsenberg et al., 2016; Cyronak et al., 2018) are beneficial for informing experimental studies about the current baseline biogeochemical variability and condition of the system. Furthermore these data may provide information about ecophysiological thresholds and the pH tolerance of organisms, including their potential acclimatization capacity to OA (Yu et al., 2011; Frieder et al., 2014). However, there is still a lack of understanding in the spatial and seasonal variability of biogeochemical parameters across nearshore ecosystems (Davidson et al., 2015). Establishing a baseline of environmental ranges and variability is the first

step to make accurate projections for the future and to guide ecological manipulation experiments targeting near-shore marine organisms and ecosystems (Andersson et al., 2015).

To accomplish this essential first task, the primary objective of this study was to characterize the temporal and spatial variability of seawater biogeochemical parameters in the SCB near-shore environment in La Jolla, CA. In particular, the study aimed to expand the current understanding of how variations in the upwelling intensity affect the biogeochemistry and OA parameters of this region. Some of the core questions to be addressed included: (i) To what extent does upwelling intensity alter seawater CO_2 chemistry in the near-shore environment?; (ii) How close to shore do upwelled low pH seawater intrude and what specific habitats are affected by this water?; (iii) How shallow in the water column do the upwelled low pH seawater reach?; and (iv) What other processes are significantly influencing the variability in seawater CO_2 chemistry in this region and to what extent? To address these questions, biogeochemical parameters were measured on a monthly transect by small-boat extending from the Scripps Pier in La Jolla to the 40 m depth contour between March 2017 and September 2018. These observations were paired with autonomous sensor measurements of seawater temperature, salinity, pH, dissolved oxygen, and currents at 18 m depth along the transect from April 2018 to November 2018. In order to understand the potential links between near-shore seawater biogeochemical variability and upwelling intensity, the data were analyzed in context of the Pacific Fisheries Environmental Laboratory (PFEL) upwelling index (https://oceanview.pfeg.noaa.gov/projects). The data were also compared to a previous study of the same area conducted in 2014 (Davidson et al., 2015).

Methods

Site description

This study was located in La Jolla, CA in the southern portion of the CCS and SCB and was conducted from March, 2017 to November, 2018 (Fig. 1). La Jolla has a Mediterranean climate and experiences relatively small amounts of rain throughout the slightly cooler winter and spring months followed by warm and dry summer and fall months (Largier et al., 1997). Seasonal variation in atmospheric winds results in the offshore movement of seawater and the upwelling of deep water into the marine system from March to September (Di Lorenzo et al., 2003). On longer time scales, the El Niño Southern Oscillation typically generates wetter, warmer, and more humid winters during El Niño phases and cooler and drier conditions during La Niña phases in La Jolla (Pavia et al., 1998).

The repeat transect for this study was located south of the Ellen Browning Scripps Pier at 32.8634° N, 117.2546° W and extended 2 km from shore. Bottom depth within the transect ranged from 7 m to 60 m, with a maximum depth at the furthest offshore station. Autonomous sensors were additionally deployed 1 km into the transect at 18 m depth. The biogeochemical variability in the study area is heavily influenced by physical forcings (Navarro et al., 2013). This is primarily due to the presence of two near-shore submarine canyons (i.e., Scripps Canyon and La Jolla Canyon) that facilitate advection of lower temperature, dissolved oxygen (DO), and pH deep water from ~ 250 m depth at the connection of the canyons up to 20 m depth in the study area (Paull et al., 2013). Furthermore, the benthic composition throughout the transect is dominated by gradually sloping sand flats with small amounts of macroalgae (Davis and VanBlaricom, 1978; Morin et al., 1985). However, within 2 km of the transect is a dense kelp forests that have been known to extend 8 km southward and 1.5 km offshore (Frieder et al., 2012). The kelp forest has been observed to influence chemistry variability within the kelp ecosystems significantly (Frieder et al., 2012; Frieder et al., 2013). Mean water circulation in the area is predominantly southward along the

shore with occasional northward shifts (Frieder et al., 2012; Fig. 2) with a semi-diurnal tidal cycle range of 1 to 2 m (https://tidesandcurrents.noaa.gov/reports.html)

Instrument deployment and sampling procedures

Autonomous instruments were deployed at 32.86508° N, 117.26302° W at 18m depth in order to capture high-resolution temporal variability of benthic biogeochemical parameters and water column velocities from April to November, 2018. The monitoring station was equipped with a SeapHOx that measured temperature, salinity, pressure, pH, and DO every 30 minutes (Martz et al. 2010). The SeapHOx consisted of a Honeywell Durafet III pH sensor (Martz et al., 2010), an Aanderaa 3826 oxygen optode, and an SBE-37 MicroCAT CTD. SeapHOx sensors were factory calibrated for temperature, DO, salinity, and pressure. In order to calibrate the pH Durafet sensor, discrete seawater samples were collected next to the SeapHOx during the sampling period for the determination of TA, DIC and pH. The calibration samples were collected via SCUBA in 250 mL corning bottles during the beginning, middle and end of each deployment to assess instrumental pH drift, and none was detected. The cross-calibrated accuracy of the pH Durafet sensor for both deployments is calculated to be ± 0.01 (Bresnahan et al., 2014). Additionally, an acoustic doppler current profiler (ADCP; Aquadopp Profiler 1 MHz, *Nortek*) collected current data every 60 seconds in 1 m bins. Starting from 0.4 m above the sensor, the ADCP sampled to a max height of 15.4 m above the sensor. The data was averaged every 10 min for the average current speed and direction across all depth bins. The instruments were secured to the seafloor on top of a Sea Spider mooring frame weighted to the benthos by 150 lbs weights and secured via 2 sand-screws. The instruments were removed once for maintenance and were frequently visited via SCUBA to collect additional, discrete seawater samples for calibration, perform routine cleaning, and make general observations.

In addition to autonomous measurements, spatial and temporal variability of seawater carbonate chemistry was assessed via discrete seawater samples using a 5 L Niskin Water Sampler (General Oceanics) and a Castaway CTD profiler (SonTek) during monthly transect surveys from March 2017 to August 2018. Samples were collected at four stations equally spaced along a transect extending from the Scripps Pier to the 60 m depth contour. The spatial sampling surveys took an average of 2 hours solely during low swell (< 1 m) conditions and encompassed four equally spaced stations along a 2 km long transect extending west from near the Ellen Browning Scripps Pier. Furthermore, samples were collected at 10 m depth intervals from the surface to 40 m depth with the exception of the station most proximal to shore where an additional sample was collected at 5 m depth. However, it should be noted that the deepest sampling depth at each station was shallower than the station's bottom depth. Samples for seawater carbonate chemistry were collected from the 5 L Niskin bottle (General Oceanics) following standard sampling protocol (Dickson et al., 2007) and preserved in 250 mL Corning Pyrex glass bottles by immediately poisoning with 100 μL saturated mercuric chloride ($HgCl_2$) (Dickson et al., 2007). An additional 30 mL of seawater from the same Niskin was then collected into a Luer-Lok syringe and 0.45 μm filtered through Millipore polycarbonate filters into 30 mL Falcon tubes and frozen for inorganic nutrient analysis. Following seawater collection, measurements of temperature (± 0.3 °C), DO (± 2 %), and salinity (± 0.1 ppt) were taken using a YSI Professional Plus handheld multi-parameter instrument (YSI 6600 V2). Salinity for the YSI was calibrated to Dickson Certified Reference Material (CRM) and DO was calibrated in 100 % saturated air at the start of each transect. Potential density was calculated using measured temperature and salinity using the MATLAB Gibbs SeaWater Oceanographic Toolbox of TEOS-10 (http://www.teos-10.org/) (McDougall & Barker, 2011). Potential densities were then subtracted by 1000 kg m^{-3} to obtain sigma theta and were used

to identify isopycnal surfaces to trace the movement of water masses through space and time in this study. Sigma theta will be used as a proxy for density and isopycnal surfaces throughout the rest of this study.

Sample analysis

All seawater carbonate chemistry samples were analyzed at the Scripps Coastal and Open Ocean Biogeochemistry lab. Seawater samples were measured for dissolved inorganic carbon (DIC) via an automated infrared inorganic carbon analyzer (AIRICA, *Marianda*) with a LI-COR 7000 as the detector. Total alkalinity (TA) was measured via a potentiometric open-cell acid titration system (0.1 N HCl) developed by the laboratory of Professor A. Dickson at Scripps Institution of Oceanography (SIO) (Dickson et al., 2007), pH was measured via spectrophotometric titrations (SAMI, Sunburst) using metacresol purple as an indicator dye. Seawater TA and DIC measurements were referenced for accuracy and precision to certified reference materials (CRMs) provided by Professor A. Dickson. Accuracy was calculated as the average offset (± 1 SD) from the CRMs. TA had an accuracy of 0.93 ± 1.40 (n = 40) and DIC had an accuracy of 0.45 ± 1.57 (n = 69). CRMs were analyzed every five samples for DIC and every ten samples for TA. Seawater pH measurements were also referenced for accuracy and precision (± 0.03 for 9 consecutive measurements at 20 °C) to TRIS buffer solutions which were used as a reference material and provided by Professor A. Dickson at SIO. The MATLAB program CO2SYS (version 2.1) (van Hueven et al., 2011) was used to calculate the seawater aragonite saturation state (Ω_{Ar}) using in situ seawater temperature, salinity, TA, and DIC as inputs. K1 and K2 dissociation constants from Mehrbach et al. (1973) refit by Dickson and Millero (1987), $KHSO_4$ dissociation constants from Dickson, and $[B]_T$ from Uppstrom (1974) were used for the CO2SYS calculations.

Dissolved inorganic nutrient samples were analyzed via a Seal Analytical continuous-flow AutoAnalyzer 3 (AA3) (Hydes et al., 2010) at the Oceanographic Data Facility at SIO using a spectrophotometer to analyze nitrate, nitrite, phosphate, and silica and a fluorometer to analyze ammonia according to each nutrient's respective standard protocol (Armstrong et al., 1967; Berhardt and Wilhelms, 1967).

Data analysis

For visualization of discrete seawater samples of both measured and calculated biogeochemical parameters, data were spatially interpolated between sampling stations for each transect and temporally interpolated between each transect for all four sampling stations using a cubic interpolation in MATLAB. Speed and direction from ADCP data were converted into U and V components and integrated throughout the water column, at the sensor station along the transect. Calibrated SeapHOx pH measurements were fitted using a smoothing spline ($p = 0.8805$) in order to highlight the dominant trend in the data set and remove some of the noise observed in the diel variability at the station. Correlation analyses of physical and chemical parameters and associated variability were conducted in MATLAB using matlab functions var and lsqfitma to determine the correlation coefficient (R) between parameters.

Upwelling variability and intensity

To approximate the variability and intensity of upwelling in the study area, daily time series upwelling index data from the Pacific Fisheries Environmental Laboratory (PFEL) were used to analyze these parameters at 33 ° N, 119 ° W (https://oceanview.pfeg.noaa.gov/projects; Fig. 1). Although these data are not specifically for the study location, they represent the most proximal upwelling station for this study. The PFEL upwelling index is based on estimates of Ekman mass transport of surface waters due to wind stress and Coriolis force (Bakun et al., 1973; Bakun et al.,

1975). Calculated upwelling indices had 1° resolution from sea level pressure fields provided by the US Navy Fleet Numerical Meteorology and Oceanography Center. Positive values on the upwelling index are interpreted as upwelled waters from underneath the Ekman layer due to equatorward wind stress in the units of m^3 s^{-1} 100 m^{-1} coastline. Negative values are interpreted as downwelling followed by onshore transport of surface waters. T-tests were conducted in MATLAB using ttest2 to determine whether there was a significant difference between yearly upwelling indexes. Upwelling intensity and biogeochemical anomalies between different years were calculated relative to observations from 2014 (Davidson, 2015). For upwelling intensity, the daily upwelling index from PFEL was averaged in 5 day segments from March to September of both 2017 and 2018 and subtracted from the reference year of 2014. For biogeochemical parameters, data were temporally interpolated on a 5 day resolution between each transect from March to September of both 2017 and 2018. These data were then subtracted from similarly represented cubic interpolated data from March to September, 2014.

Results

Temporal variability from autonomous sensor data

La Jolla experienced semidiurnal tides that throughout the sensor deployment period had an average tidal amplitude of 1.58 ± 0.37 m (Fig. 3). The measured amplitude of spring tides was 1.84 ± 0.28 m while neap tides experienced an amplitude of 1.24 ± 0.18 m. Primarily, the depth integrated current direction paralleled the coast, flowing either in a south-southwesterly or north-northeasterly direction, with a water column integrated speed ranging from 2 to 25 cm s^{-1} and an average of 6 ± 3 cm s^{-1} (Fig. 2).

In general, average seawater temperature from the SeapHOx at 18 m depth was lowest between April to mid-June (13.5 ± 1.6 °C) and then gradually increased to mid-August (Fig. 3). The average temperature between mid-August and November was 16.4 ± 1.3 °C. However, large daily and weekly variations of up to 8.7 °C and 9.4 °C, respectively, were prominent throughout the deployment period. Despite visual trends in the daily range (midnight to midday) of temperature values, the variability was not statistically correlated with the tidal amplitude (R^2 = 0.0929, $p > 0.05$), where larger temperature variability would be associated with larger tidal amplitude and smaller variability associated with smaller tidal amplitude (Fig. 3). Inter-weekly diel mean range was similar between April to August (5.47 ± 1.20 °C) and August to December (5.62 ± 1.30 °C) despite the difference in average temperatures (Table 1).

Salinity was relatively consistent with a daily average of 33.4 ± 0.2 between April and mid-June followed by a decrease to 33.1 ± 0.1 until the end of July. It then increased and remained fairly constant until the end of the year (33.4 ± 0.1 p) (Fig. 3).

On average, pH was lower from April to August (7.85 ± 0.07) compared to August to November (8.00 ± 0.04). Through mid-April to mid-May, pH experienced relatively stable mean daily values with an average pH of 7.82 ± 0.03. At the end of May there was an increase in pH to 8.02 followed by a sharp decrease to 7.68 and a return to a higher pH of 7.90 after several days (Fig. 3). This drop in pH coincides with a drop in DO to near-zero concentrations. Following this event, pH continued to decrease from the end of May to mid-June where the lowest pH of 7.64 was observed. From mid-June to mid-August pH, two more events were observed starting with an initial increase to 7.95 and followed by a decrease back down to 7.69 (Fig 3). From then on pH remained relatively constant with an average of 8.00 ± 0.04. Throughout April to November the daily average pH range was 0.09 ± 0.04; however, larger daily and weekly variabilities of up to

0.22 and 0.47, respectively, were observed throughout the deployment. Similar to temperature, pH amplitude was not statistically correlated with the tidal amplitude ($R^2 = 0.0030$; $p > 0.05$).

DO followed the same overall trend of pH with lower mean values from April to early-August and higher mean values from mid-August to November (150 ± 24 μmol kg^{-1} and 222 ± 14 μmol kg^{-1}, respectively). The daily variability was larger from April to early-August (80 ± 31 μmol kg^{-1}) compared to early-August to November (32 ± 14 μmol kg^{-1}). The maximum and minimum daily variability were observed in June (139 μmol kg^{-1}) and October (10 μmol kg^{-1}), respectively. Temperature and DO were positively correlated ($R^2 = 0.6710$, $p < 0.001$) with low temperatures coinciding with low DO concentration and high temperatures having higher DO concentrations, especially in the time-frame from mid-April to early-August (Fig 3). Furthermore, there was large daily variability in temperature, pH, and DO that ranged from 11.2 to 19.9 °C, 7.66 to 7.88, and 122 to 261 μmol kg^{-1}, respectively, with lower temperature, lower pH, and lower DO waters observed from April to August and higher values during the later months of August to November (Fig 3).

Spatiotemporal seawater carbonate chemistry variability

Seawater temperature always decreased with depth except for in December, 2017 when a uniform temperature was observed from the surface to 40 m depth. The largest temperature range during any one sampling event occurred during July 2018 with a surface temperature of 25.9 °C and a bottom temperature of 13.4 °C . This coincided with one of the highest temperature ever measured off of the Scripps Pier (https://scripps.ucsd.edu/news/highest-ever-seawater-temperature-recorded-scripps-pier). Similarly, the maximum surface seawater temperature and largest range between surface and bottom in 2017 also occurred in the month of July. In contrast, the lowest temperatures measured at 40 m depth were found between April-June with temperatures

as low as 10.5 °C (Fig 4). Throughout the winter months of December to February, the water column was well-mixed with an average temperature of 15.5 ± 0.6 °C and a range of 3.8 °C between the four sampling transects (Fig 4). In comparison, the months of April to November displayed a strongly stratified water column with average temperatures of 15.9 ± 3.6 °C (range = 13.8 °C) and 17.5 ± 3.4 °C (range = 14.8 °C) during 2017 and 2018, respectively, (Fig 4).

In terms of seawater chemistry, DIC, pH, Ω_{Ar} and DO followed the spatial and temporal variability in seawater temperature. High DIC, low pH, Ω_{Ar} and DO coincided with low seawater temperature at depth while the opposite was observed in conjunction with high temperature at the surface (Fig 5-8; Fig 10). TA on the other hand showed less of a correlation with these parameters and was relatively constant throughout the study period although slightly higher TA (2245 ± 9 μmol kg^{-1}) was typically observed in the summer months at both the surface and bottom. The average TA (± SD) throughout the water column for the entire study period was 2236 ± 10 μmol kg^{-1} (Fig 9). The largest vertical ranges in DIC, pH, Ω_{Ar} and DO mostly coincided with the largest ranges in temperature, and occurred in either June of 2017 or July 2018, respectively (Table 2). The extreme low values of DIC, and high values of pH, Ω_{Ar} and DO observed at the surface were 1806 μmol kg^{-1}, 8.29, 4.75, and 345 μmol kg^{-1}, respectively, whereas opposite extreme values at depth were 2193 μmol kg^{-1}, 7.69, 0.93, and 125 μmol kg^{-1}. In contrast, the lowest vertical variability of these parameters were observed in December 2017 and coincided with a well-mixed water column observed during that survey (Table 2). In comparison to vertical gradients, horizontal variability across any particular depth during a single transect was relatively small for DIC, pH, Ω_{Ar}, and DO. For example, average surface DIC variability throughout each transect was 12 ± 7 μmol kg^{-1} (mean ± SD; n = 19 for each individual survey) in comparison to vertical gradients of 150 ± 71 μmol kg^{-1}. However, while there was limited surface variability in biogeochemical

parameters across a given transect, there were comparatively larger differences in the average surface values between months. In one case, by comparing average surface values in DIC from June (1944 ± 6 μmol kg^{-1}) to July (1815 ± 15 μmol kg^{-1}) of 2017, we observed a 129 μmol kg^{-1} decrease in surface water DIC. Similarly, pH, Ω_{Ar}, and DO experienced low horizontal spatial variability in a single transect but underwent large temporal variability with the greatest month-to-month surface value decrease of 0.20, 1.31, and 61 μmol kg^{-1}, respectively, from July to August, 2017, and the greatest month-to-month surface increase of 0.20, 1.51, and 53 μmol kg^{-1}, respectively, from June to July, 2017.

Similar to CO_2-chemistry parameters and oxygen, most dissolved inorganic nutrients (i.e., silica [SiO_2], nitrate [NO_3^-], and phosphate [PO_4^{3-}]) followed trends in seawater temperature with high concentrations ([SiO_2] = 23.9 μmol kg^{-1}, [NO_3^-] = 23.6 μmol kg^{-1}, [PO_4^{3-}] = 1.9 μmol kg^{-1}) coincident with low seawater temperature and isopycnal surfaces with a sigma theta greater than 25 kg m^{-3}. In contrast, the average concentration of silica, nitrate, and phosphate at the same depth was lower in the winter months (December to February) and were 3.8 ± 1.0 μmol kg^{-1}, 2.6 ± 1.2 μmol kg^{-1}, and 0.5 ± 0.1 μmol kg^{-1}, respectively. (Fig 11-13). Although variations in [SiO_4], [NO_3^-], and [PO_4^{3-}] were strongly correlated, nitrite [NO_2^-] and ammonia/ammonium [NH_3/NH_4^+] showed radically different variabilities. Elevated [NO_2^-] coincided with increases in other dissolved nutrients in spring, but then drastically decreased in the middle of summer before increasing again in the late summer or fall (Fig 14). In contrast, [NH_3/NH_4^+] showed no distinguishable trend throughout the study period (Fig 15).

Upwelling intensity and anomalies

During the study period, the Upwelling Index (UI) measured in m^3 s^{-1} 100 m^{-1} coastline calculated by NOAA PFEL (https://oceanview.pfeg.noaa.gov/projects) revealed lower intensity

and variability during the fall and winter months, and higher intensity and variability from April to August (Fig 16). In 2017, the total amount of upwelling between March and October equaled ~2.7 x 10^9 m^3 100 m^{-1} with an average of 129 ± 83 m^3 s^{-1} 100m^{-1} at the 33 ° N, 119 ° W, PFEL station. A similar value was observed in 2018 of ~2.6 x 10^9 m^3 100 m^{-1} and an average of 125 ± 70 m^3 s^{-1} 100m^{-1} at the same station. Statistically, these values were not significantly different ($p > 0.05$). Variations in seawater temperature and biogeochemical parameters closely tracked the seasonal variation in upwelling intensity, which were strongly driven by the intrusion of cold, high CO_2, and low oxygen waters (Figs 16 and 17). The range of pH and Ω_{Ar} exposure were similar at 20, 30, and 40 m depths, ranging from 7.69-8.06 and 0.93-2.50, respectively, but with decreasing mean conditions as a function of increasing depth. In contrast, the mean and the range of pH (7.86-8.25) and Ω_{Ar} (1.5-4.5) exposure sequentially increased at 10 m and at the surface compared to deeper depths (Figs 18 and 19). Furthermore, the deepest depth illustrated the highest percent of observations of lower Ω_{Ar} and pH values. Where at 40 m, 50 % of the time Ω_{Ar} values were < 1.5 and 35 % of the time pH values were < 7.82 (Figs 18 and 19). The duration of exposure and intensity decreased with shallower depth, however, exposure to near or undersaturated seawater was still observed in the 20 to 40 m depth bins for up to 10 % of the time (Figs 18 and 19). In comparison, at the top 10 m of the water column, 90 % of the time Ω_{Ar} was > 1.8 and 95 % of the time pH was > 7.95 (Figs 18 and 19).

In order to better understand the results from 2017-2018, the observations from these years were compared to similar data collected in 2014 (Davidson, 2015). Comparatively, 2014 experienced a lower average upwelling (99 ± 63 m^3 s^{-1} 100m^{-1}) and a lower total amount of upwelling (~2.0 x 10^9 m^3 100 m^{-1}) between March to October compared to 2017 and 2018. Comparison of isopycnal surfaces for the upwelling seasons of 2014, 2017, and 2018 (Fig 20), in

terms of sigma theta (sigma theta = calculated density – 1000 kg m^{-3}) showed that the 25 kg m^{-3} isopycnal surface reached depths between 10-20 m depth between mid-March to mid-July with some variations in timing and intensity between these years. The 25 kg m^{-3} isopycnal surface reached shallower depths earlier in 2014 and 2018 compared to 2017, and also remained at shallower depths for a longer duration in 2014 compared to 2018. Furthermore, in 2014, denser water (25.6 kg m^{-3}) was observed to penetrate to shallower depth (25 m) than in 2017 and 2018. In fact, this isopycnal surface was only marginally observed at 40 m depth in 2017 and not observed at all in 2018. However, it should be noted that these observations were based on monthly measurements and may be missing higher frequency variability.

Overall, variations in seawater physical and biogeochemical parameters were strongly correlated with isopycnal surfaces, with cold temperatures, high DIC and dissolved inorganic nutrients, low pH, Ω_{Ar} and DO observed alongside the denser isopycnals (Figs.4-8, 11-13). This was consistently observed for all years of observations and provided clear evidence of a deep-water origin. However, one important question of interest is whether differences in the upwelling intensity or the origin of the upwelled water (as indicated by density) produced distinct differences in pH and Ω_{Ar} between the different years. For example, did the higher upwelling intensity observed in 2017 and 2018 produce overall lower pH and Ω_{Ar} conditions compared to 2014, or did the intrusion of denser water to shallower depth in 2014 have the same effect?

In 2017, the water below 20 m was in general less dense between March and May and more dense between May and mid-July compared to 2014 (Fig. 20 and 21). Both pH and Ω_{Ar} anomalies were inversely correlated to the density anomalies (Fig 21A-C), i.e., if the density was lower compared to 2014, the pH and Ω_{Ar} were higher, and if the density was higher, the pH and Ω_{Ar} were lower. Positive anomalies of pH and Ω_{Ar} observed before May were up to 0.07 and 0.25 units

higher in 2017 compared to 2014, whereas negative anomalies observed after May were up to 0.25 and 1.0 units lower (Fig 21B-C). In contrast to 2017, most of the water column in 2018 was less dense compared to 2014 as indicated by negative density anomalies (Fig 20 and 21). In terms of pH and Ω_{Ar}, both parameters were mostly higher in 2018 compared to 2014, except from mid-June, below 10 m, where lower pH and Ω_{Ar} values of -0.15 and -0.7 units were observed. These negative pH and Ω_{Ar} anomalies did not coincide with a positive density anomaly, but roughly coincided with strong positive anomalies in the top surface layer most likely associated with a plankton bloom. It is possible that organic material originating from this bloom were subsequently remineralized at depth and responsible for the negative pH and Ω_{Ar} anomalies.

Discussion

Spatiotemporal variability of biogeochemical parameters

Temporal variability

Diel variability (± SD) of seawater temperature, pH and DO was highly variable throughout the survey (4.4 ± 1.6 °C; 0.10 ±0.04; and 58 ± 23 μmol kg^{-1}, respectively). The variability in these parameters was driven by a combination of the diel light cycle and advection of different water masses linked to the tidal cycle and upwelling events as has been reported from other studies in the same area (Frieder et al., 2012; Takeshita et al., 2015). Diel variability in pH and DO was primarily driven by photosynthesis and respiration by organisms in the water column similar to geographically related study sites (Hofmann et al., 2011; Frieder et al., 2012; Takeshita et al., 2015; Kapsenberg et al., 2016; Silbiger et al., 2018). Although the average diel pH and DO ranges were 0.10 ± 0.04 and 58 ± 23 μmol kg^{-1}, respectively, maximum ranges of 0.24 and 210 μmol kg^{-1}, and minimum ranges of 0.02 and 13 μmol kg^{-1}, were observed. The difference in magnitude of

the diel variability in pH and DO was likely linked to variations in light availability, biomass, rates of photosynthesis and respiration, nutrient availability, and also influenced by hydrodynamics.

Seawater temperature, salinity, pH and DO also displayed weekly to seasonal variability, with temperature, pH and DO lower from April to July and then higher between the months of August to November. This variability was likely driven by seasonal differences in light and water column productivity as well as localized physical processes related to the tidal cycle, upwelling and advection of chemically modified water masses from nearby habitats (e.g., kelp forest; Frieder et al., 2012; submarine canyons; Swart et al., 2011; Navarro et al., 2013; Takeshita et al., 2015). Furthermore, these longer timescale processes probably also influenced the diel variability of the system, such as, nutrient rich, upwelled waters increasing the diel productivity of the system which also could lead to subsequent increased respiration. A large drawdown in pH and DO to nearly anoxic conditions in May, 2018, may be indicative of substantial decomposition of organic matter at the study site, but seems unlikely, and is most likely indicative of a temporary clog or blockage in the SeapHOx pump that eventually cleared. These data should be considered as erroneous data.

Spatial variability

Variations in the upwelling intensity was the primary source of seasonal spatiotemporal variability in seawater biogeochemical parameters. This seasonal variability was observed in both autonomous sensor data and discrete seawater samples, however the majority of variability was observed in the vertical direction during individual transects from discrete seawater samples. From March to August of both years, more consistent, strong upwelling events advected nutrient rich, low pH, Ω_{Ar}, DO, and temperature water towards the shore (Table 2; Figs 3-9 and 11-15). The advection of upwelled waters increased the stratification in the system and exposed the near-shore system to low pH and occasionally undersaturated ($\Omega_{Ar} < 1$) or nearly undersaturated ($1 < \Omega_{Ar} <$

1.2) seawater (Fig 7) for consecutive months from April to July, 2017 and March to May, 2018. Peak upwelling occurred in either May or June of both years and was associated with the lowest observed pH and Ω_{Ar} values and the highest nutrient enrichment (Figs 6-7 and 11-15). Additionally, this increase in upwelling coincided with the lowest observed Ω_{Ar} (0.93) that was observed as shallow as 20 m during the month of June, 2017. Overall, presence of nearly undersaturated seawater was observed as shallow as 20 m, during any single survey, and persisted throughout multiple months of both years. While undersaturated seawater has been observed in similar shallow depths in the northern regions of the CCS (Feely et al., 2008; Harris et al., 2013; Hauri et al., 2013), it has never been documented as shallow as 30 m or within 2 km of the shore in the San Diego area or greater SCB (Feely et al., 2009; Leinweber et al., 2013). Furthermore, we also observed the largest shoaling of upwelled waters, indicated by increased nutrient concentrations and low pH and Ω_{Ar} values, to depths as shallow as 10 m and within 1 km of the shore during this time frame. The results indicate that the near-shore system of the SCB experiences seasonal exposure to low seawater pH and Ω_{Ar} levels that multiple lab experiments suggest have deleterious effects to local marine organisms and ecosystem (Yu et al., 2011; Frieder et al., 2014; Silbiger et al., 2018). It is currently not known whether this is the case in the natural environment and is a topic that requires attention.

Following relaxation of the upwelling intensity in the fall, a decrease in nutrients and an increase in pH, Ω_{Ar}, DO, and temperature were observed from the months of September to November (Table 2; Fig 3-9; Fig 11-15). During the winter months (November to March), the system was characterized by a well-mixed water column with little spatiotemporal variability throughout the top 40 m for all analyzed biogeochemical parameters.

Effect of upwelling intensity

Overall, upwelling intensity varied on a seasonal basis with increasing intensity observed from March to July and decreasing intensity from August to October. During the winter months from November to February, the water column was well-mixed with no vertical gradients. Accompanying the higher upwelling intensity, lower temperature, DO, pH, and Ω_{Ar}, and higher DIC and inorganic nutrients were observed beneath the thermocline. These trends in biogeochemical parameters are strongly indicative of water with a deeper origin and the influence of seasonal upwelling. The presence of upwelled waters was most prevalent between 20 and 40 m depth, which experienced the longest exposure to lower Ω_{Ar} and pH values. This means that during peak upwelling season, habitats and marine organisms located at 20 m depth in La Jolla, i.e., kelp forests, sand dollar beds, oysters, sea urchins, lobsters, mussels, and coralline algae, are exposed to seawater near-undersaturation or even undersaturated with respect to aragonite for extended periods of time (Frieder et al., 2012; Takeshita et al., 2015). Previous studies suggest that exposure to undersaturated seawater may have direct deleterious effects on marine organisms' physiology (Pauly et al., 2002; Yu et al., 2011; Frieder et al., 2013; Feely et al., 2016; Silbiger et al., 2019) and also possibly decrease recruitment success under these conditions (Yu et al., 2011; Kroeker et al., 2011; Frieder et al., 2014). Furthermore, to our knowledge these low levels of Ω_{Ar} and pH have previously not been reported at such a shallow depth and so close to shore (< 1 km) in the southern region of the CCS. Instead these observations are more comparable to observations in Oregon and other northern regions of the CCS where upwelling intensity is stronger (Feely et al., 2008; Wooton et al., 2008; Hauri et al., 2013; Harris et al., 2013) or in deeper and more offshore stations of the CCS (Hauri et al., 2013; Feely et al., 2016; Woods et al., 2017; Thompson et al., 2018). Concurrent with climate change, it is anticipated that Ω_{Ar} and pH values could decrease even more and persist

for longer duration and at shallower depth due to increasing upwelling favorable winds transporting more water from depth to the surface (Iles et al., 2012; Wang et al., 2015)

However, while we observed correlation between the seasonal variability of upwelling intensity to variation in seawater biogeochemical parameters, we did not observe a direct correlation between specific upwelling events and variation in temperature, pH and DO from temporal data (Fig. 3). For example, in late April, 2018, an intense upwelling event (up to 325 m^3 s^{-1} $100m^{-1}$) occurred and was followed by a drawdown of seawater temperature, from 15 °C to 10 °C, and DO, from 230 μmol kg^{-1} to 95 μmol kg^{-1} (Fig 3). However, the lowest temperature and DO values associated with this specific upwelling event, lagged the peak of upwelling by approximately one week, i.e., the minimum DO and temperature occurred one week after peak upwelling. This lag between upwelling intensity and seawater temperature and DO variability was probably due to the difference in locations between La Jolla and the site of upwelling intensity calculation at 33 ° N, 119 ° W. Further analyses using cross-correlation with hydrodynamic models and our data will be necessary to assess the consistency of this lag. Since the actual upwelling occurs at the shelf break, observations in the near-shore environment reflect advection of upwelled water that could have taken multiple pathways, and thus, produce a variable lag. However, the presence of deep submarine canyons around the study site, these could act as "short-circuits" for deep water to make it to the near-shore environment (e.g., Navarro et al., 2013).

Based on the current rate of atmospheric CO_2 increase, we hypothesize that variations in the upwelling intensity is a more prominent driver of seawater biogeochemical variability in EBUS and a more critical factor to consider in terms of the success of marine organisms in these environments. By comparing observations from this study in 2017 and 2018 with measurements from 2014 (Davidson et al., 2015), we were able to get a first preliminary insight to how variations

in the upwelling intensity affect biogeochemical parameters in the near-shore environment. Our initial calculations demonstrated that both 2017 and 2018 experienced higher total amounts of upwelling in comparison to 2014. Despite this, results showed that both 2017 and 2018 did not experience overall lower pH and Ω_{Ar} levels in comparison to 2014 as we hypothesized. However, importantly, despite higher intensity in 2017 and 2018, the density of upwelled seawater was not higher compared to 2014, indicating a shallower origin. Consistently, lower pH and Ω_{Ar} levels were always coincident with higher density values suggesting that the source of the upwelled water is more important than the total amount. The only exception to this was the anomaly in June to August of 2018, which possibly was linked to a surface bloom and subsequent remineralization of organic matter at deeper depths.

In summary, the results illustrate that there are complex dynamics associated with upwelling and advection of seawater into the nearshore marine environment of La Jolla, which may be influenced by the presence of submarine canyons (Navarro et al., 2013) and propagation of internal waves (Lucas et al., 2011; Booth et al., 2012). This warrants a more in-depth understanding of the transport of water masses from the shelf to the nearshore environment, which was not the focus of this study. Furthermore, the results illustrate the wide spatiotemporal range of seawater biogeochemical conditions, which are already outside the mean global changes in surface seawater CO_2 chemistry expected by anthropogenic CO_2 emissions and resulting ocean acidification during the 21st century.

Conclusions

This study indicates that upwelling intensity is a primary driver for seasonal spatiotemporal variability of seawater CO_2 chemistry parameters in the near-shore environment of the SCB. The data show that marine habitats and organisms in this environment are at times exposed to low pH

(7.69) and seawater undersaturated with respect to aragonite, conditions that are typically expected at deeper depths or in more intense upwelling regions of the CCS. In particular, intrusion of upwelled deep waters was observed for several months during the upwelling season between March and July, extending to depths as shallow as 20 m and within 1 km of the shoreline. These observations are important for the OA research community to better understand how local marine organisms and habitats might be affected by low pH and Ω_{arag} conditions, and how seawater CO_2 chemistry variability may be exacerbated by ongoing OA. This information will be critical to ecophysiological studies aimed at developing an understanding of acclimatization and susceptibility of marine organisms and habitats, which is of relevance to many stakeholders including local fishermen and resource managers. Furthermore, the data suggest that current models and projections are underestimating the current seawater aragonite levels and possibly the rate of decline of aragonite within the CCS (Feely et al., 2008; Gruber et al. 2002; Hauri et al., 2013; Feely et al., 2016). This study can help fill this knowledge gap of near-shore seawater biogeochemical variability and for improving the development of high resolution and more accurate models. We also note that while upwelling is a primary driver of biogeochemical variability in the SCB, the upwelling intensity calculated for the shelf break at 33 ° N, 119 ° W is not a reliable indicator in predicting the duration and intensity of low pH and Ω_{Ar} seawater in the near-shore environment in La Jolla. In order to better understand the links between upwelling at the shelf break and near-shore environments, more in-depth knowledge of the local circulation and hydrodynamics is required. This includes knowledge of the role of submarine canyons that may act as a short-circuit between deep water and near-shore habitats. Finally, we conclude that the near-shore environment in SCB is already exposed to extreme seawater pH and Ω_{Ar} conditions,

and large natural variability. To properly understand how anthropogenic CO_2 will affect near-shore marine systems in the future, we first need to understand the effects of these current conditions.

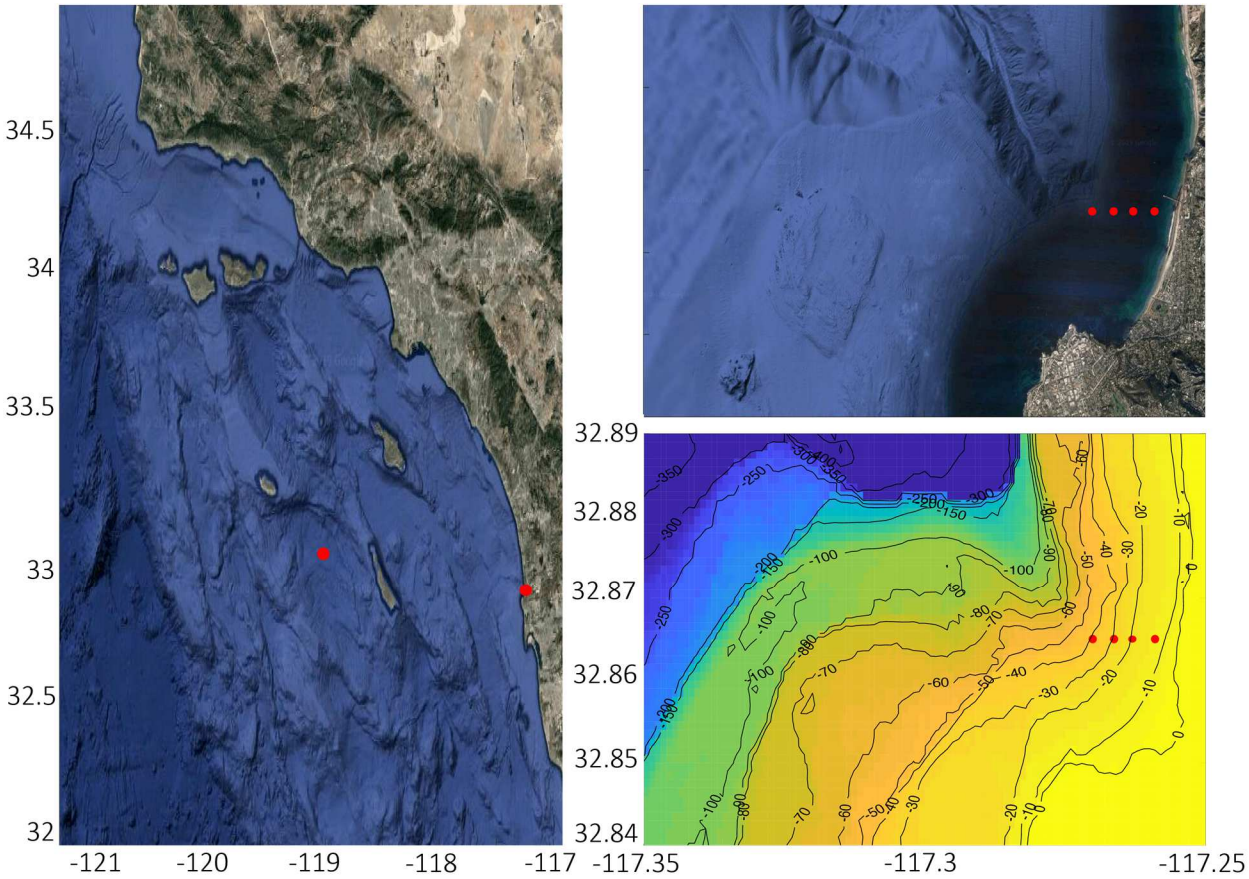

Figure 1. Map showing the location of (A) the PFEL, UI site, (B) La Jolla, and (C) the transect with respect to bathymetry.

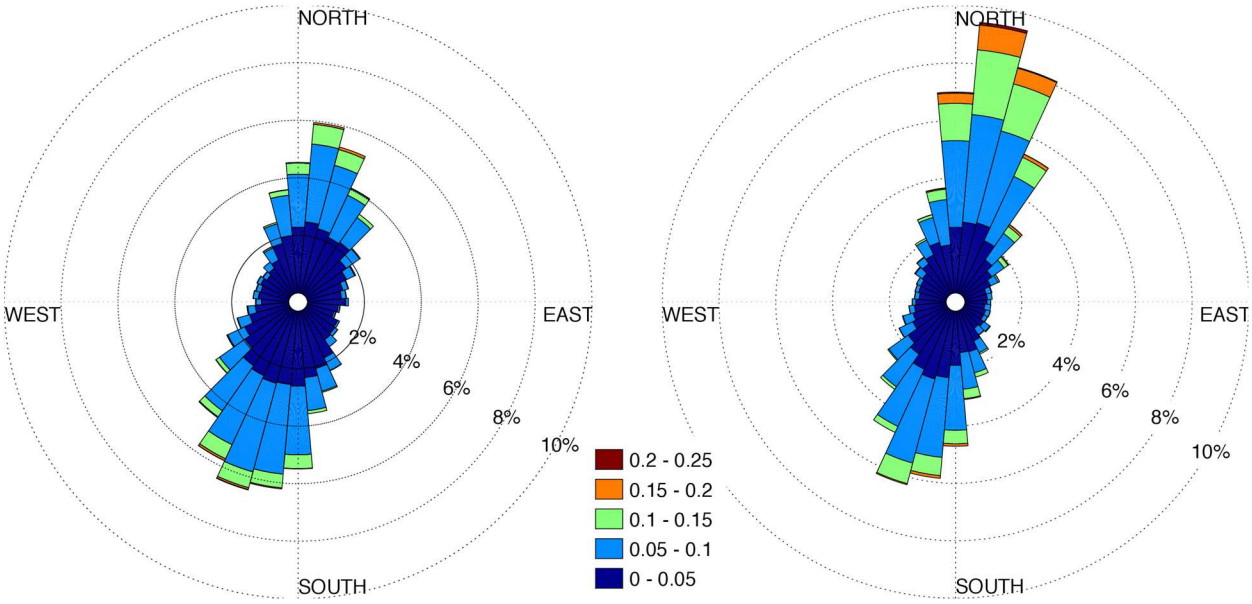

Figure 2. Current rose diagrams from the two separate deployments showing the direction of the current and the ranges in speed. Dotted circles indicate the percentage of time during which the currents measured fell in each speed and direction bin.

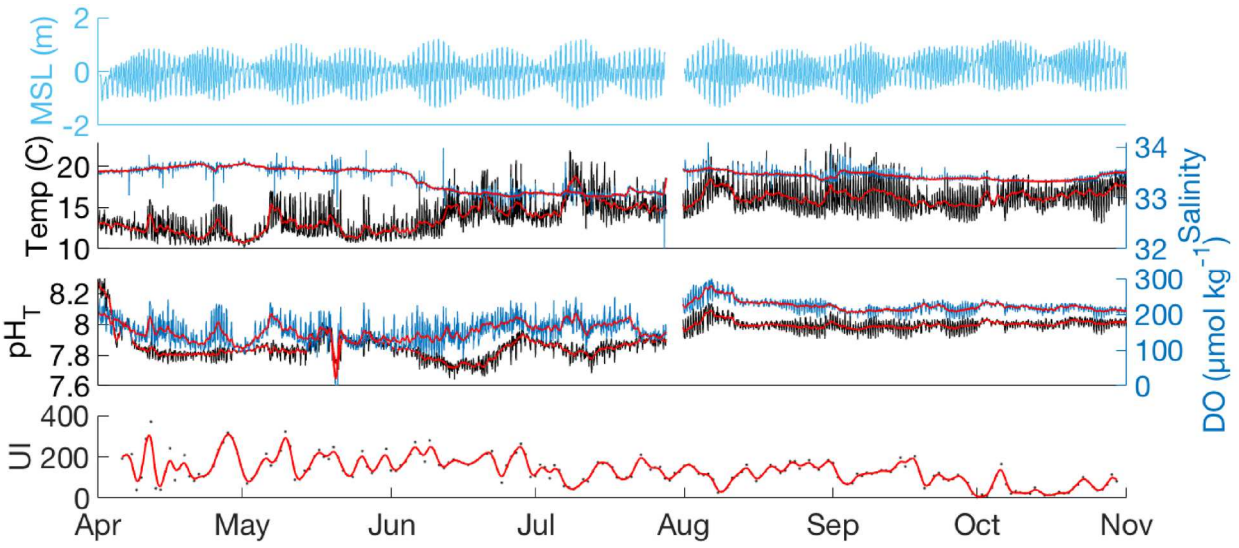

Figure 3. Temporal variability at 18 m depth of pH, dissolved oxygen, temperature, and salinity in relation to upwelling intensity and mean sea level variations from April to November, 2018. Red lines signify the spline filtered data (p = 0.8805) of each respective parameter.

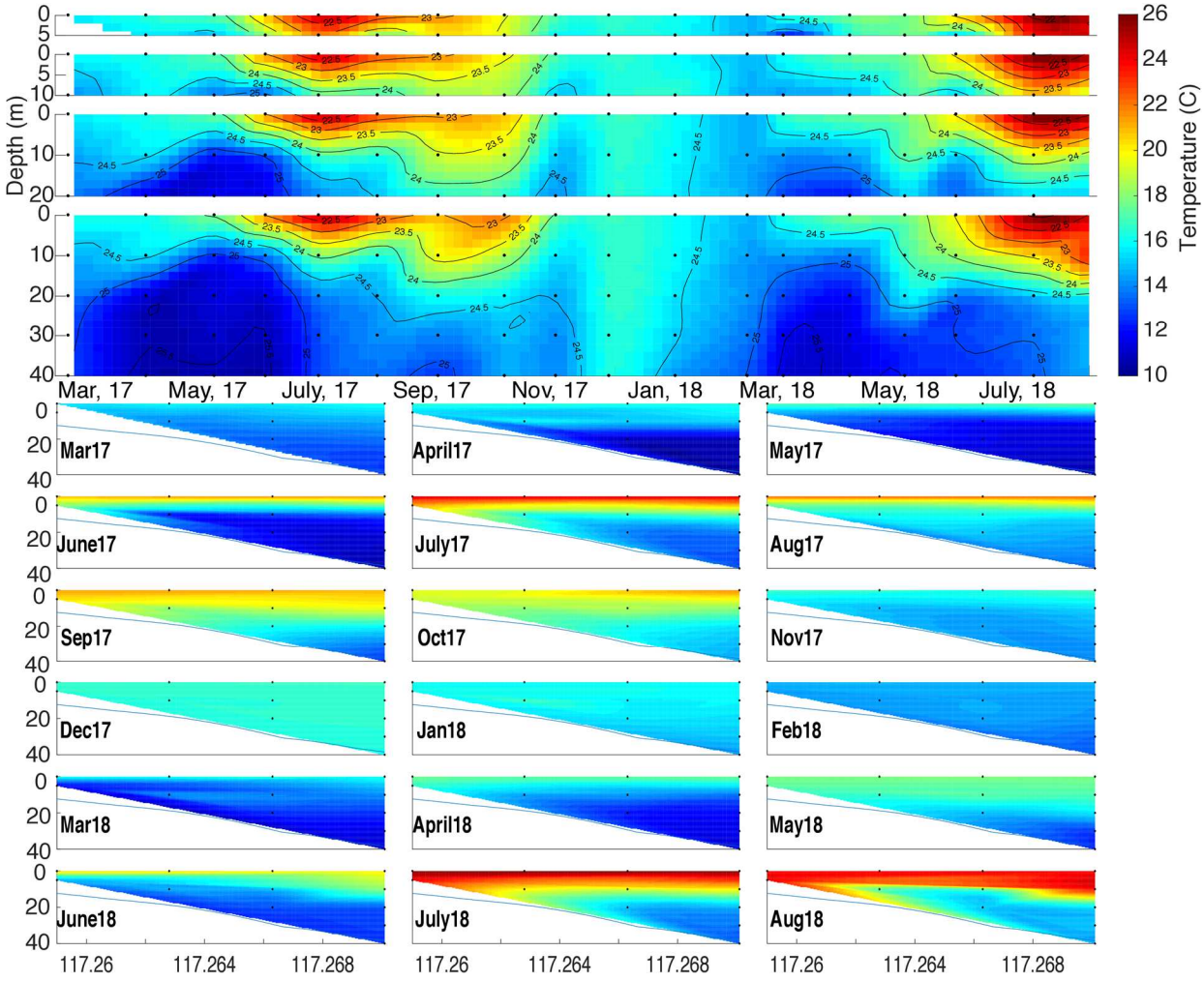

Figure 4. Spatial contour plots from gridded interpolations (cubic interpolations using MATLAB griddata) of temperature through time at each station and across each transect. The top most plot of the four plots is the most near-shore station while the lowest plot is the most offshore station. The black contour lines represent calculated isopycnals and the black dots indicate depth of discrete samples. The blue line depicts interpolated bottom depth.

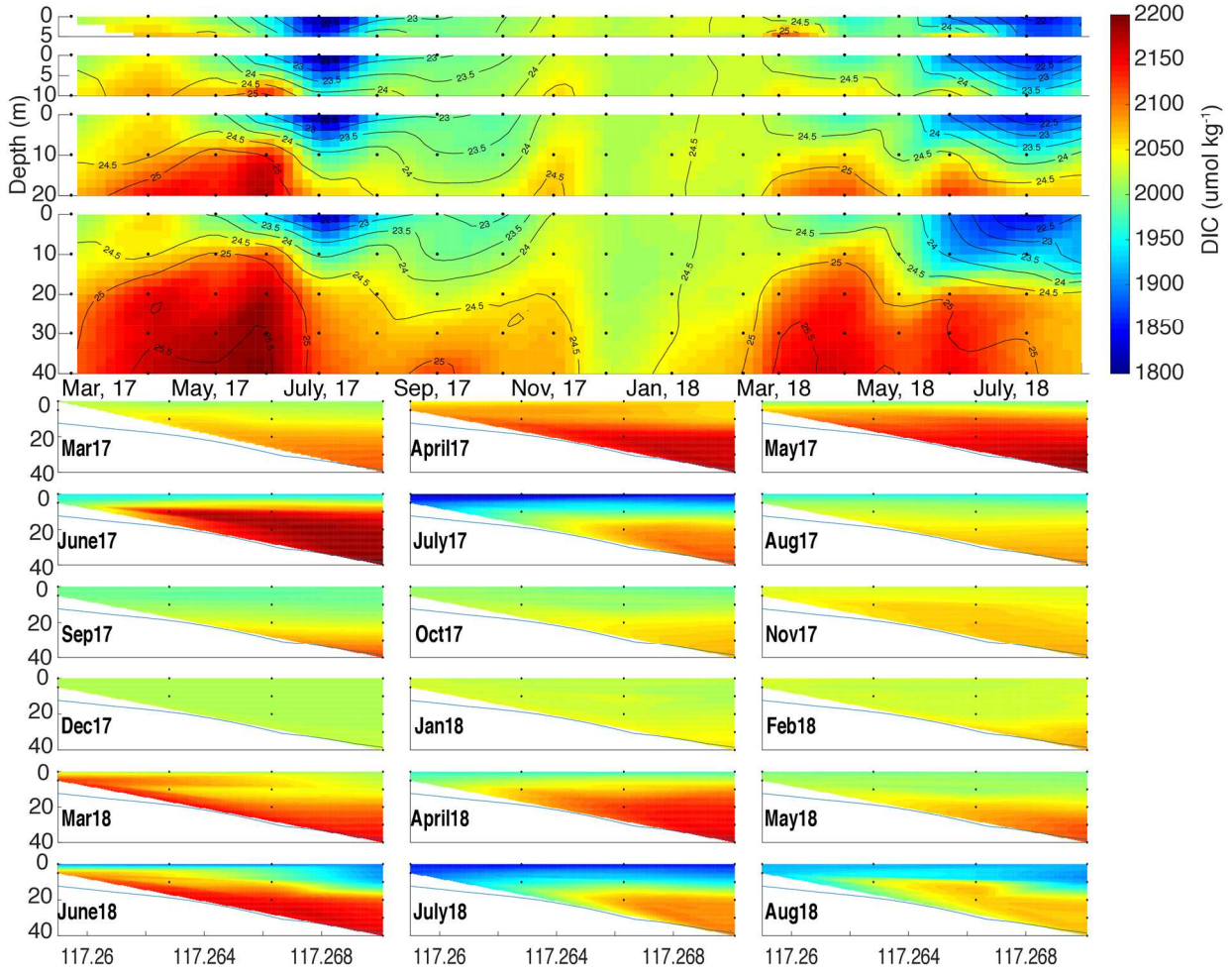

Figure 5. Spatial contour plots from gridded interpolations (cubic interpolations using MATLAB griddata) of DIC through time at each station and across each transect. The top most plot of the four plots is the most near-shore station while the lowest plot is the most offshore station. The black contour lines represent calculated isopycnals and the black dots indicate depth of discrete samples. The blue line depicts interpolated bottom depth.

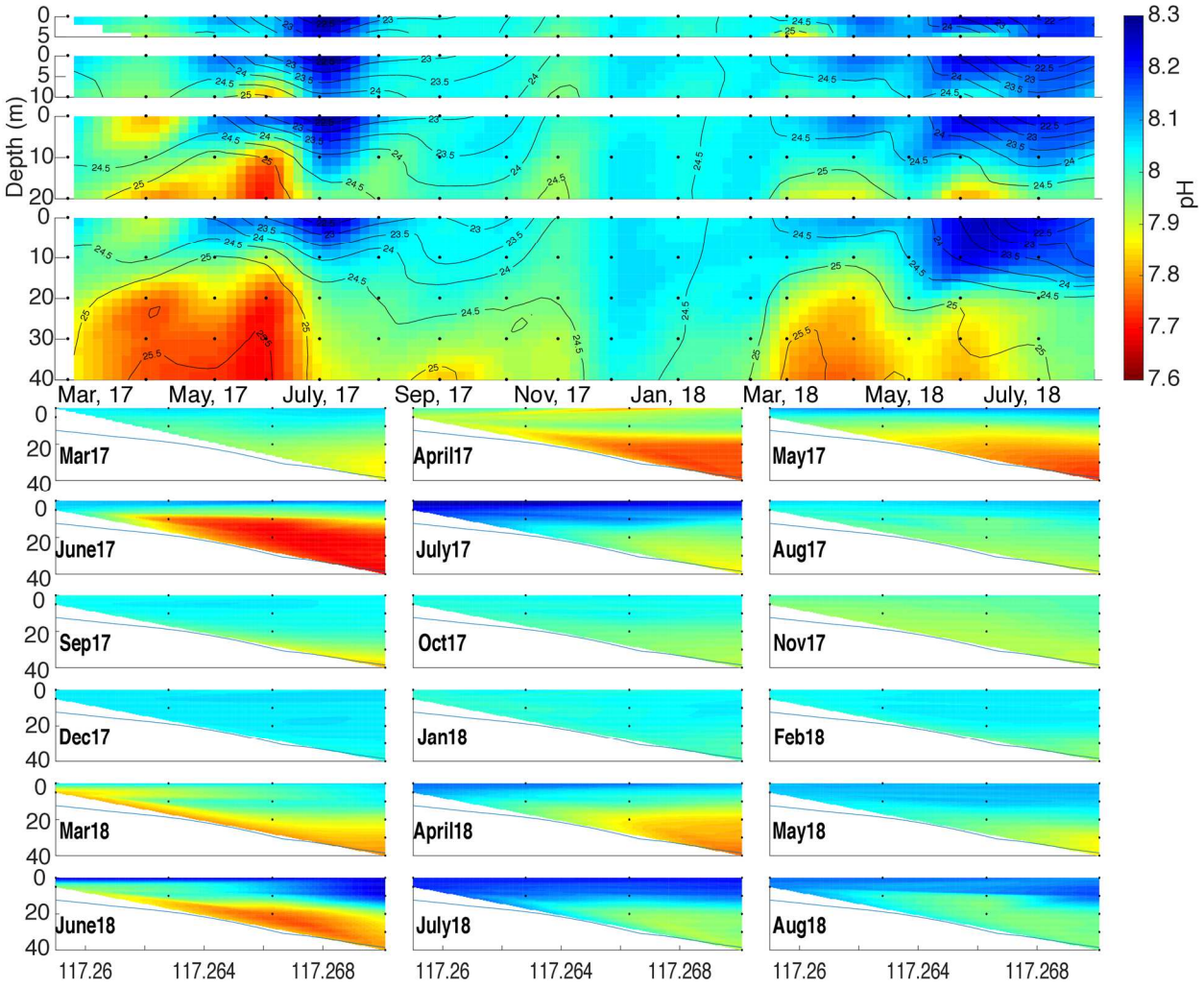

Figure 6. Spatial contour plots from gridded interpolations (cubic interpolations using MATLAB griddata) of pH through time at each station and across each transect. The top most plot of the four plots is the most near-shore station while the lowest plot is the most offshore station. The black contour lines represent calculated isopycnals and the black dots indicate depth of discrete samples. The blue line depicts interpolated bottom depth.

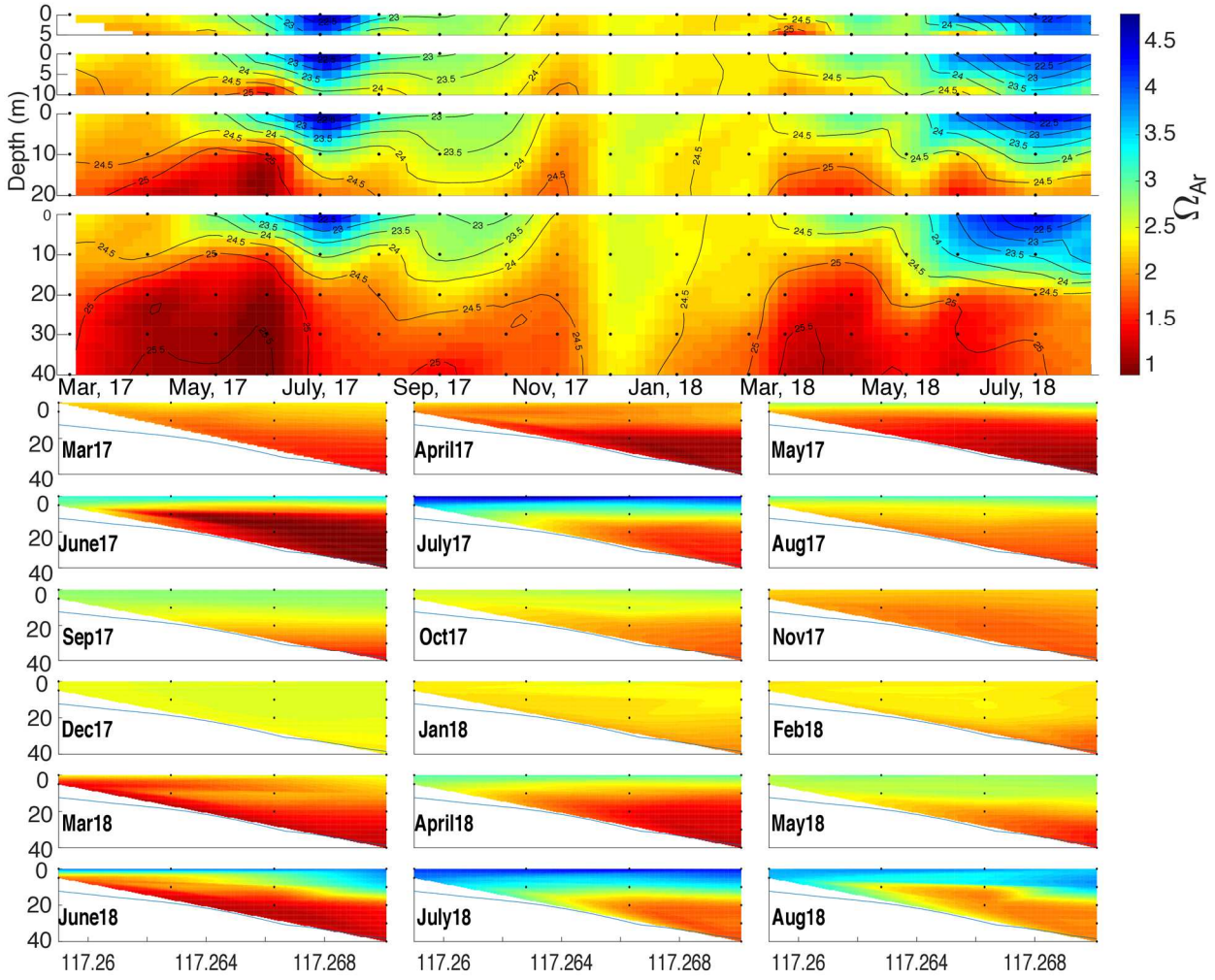

Figure 7. Spatial contour plots from gridded interpolations (cubic interpolations using MATLAB griddata) of Ω_{Ar} through time at each station and across each transect. The top most plot of the four plots is the most near-shore station while the lowest plot is the most offshore station. The black contour lines represent calculated isopycnals and the black dots indicate depth of discrete samples. The blue line depicts interpolated bottom depth.

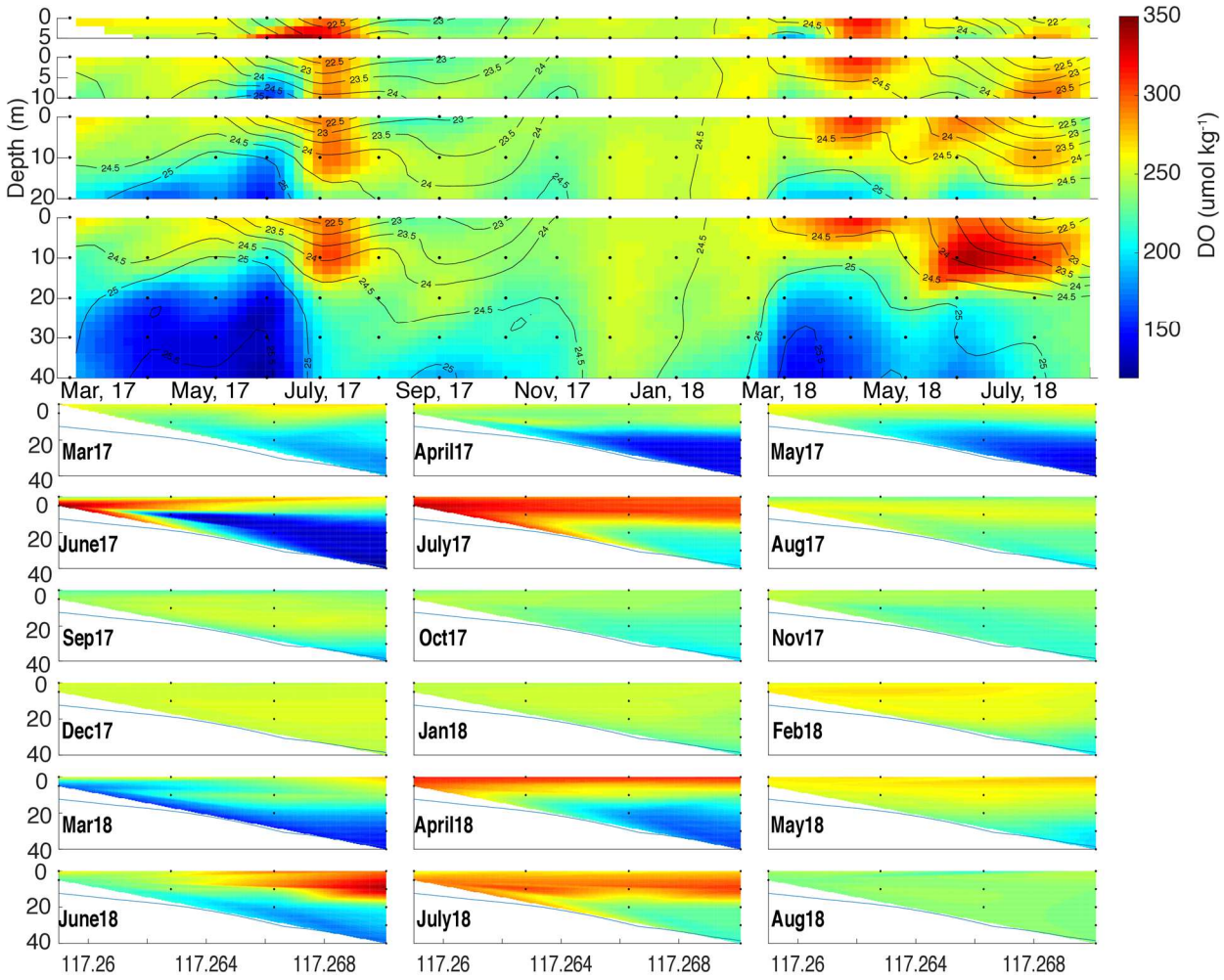

Figure 8. Spatial contour plots from gridded interpolations (cubic interpolations using MATLAB griddata) of DO through time at each station and across each transect. The top most plot of the four plots is the most near-shore station while the lowest plot is the most offshore station. The black contour lines represent calculated isopycnals and the black dots indicate depth of discrete samples. The blue line depicts interpolated bottom depth.

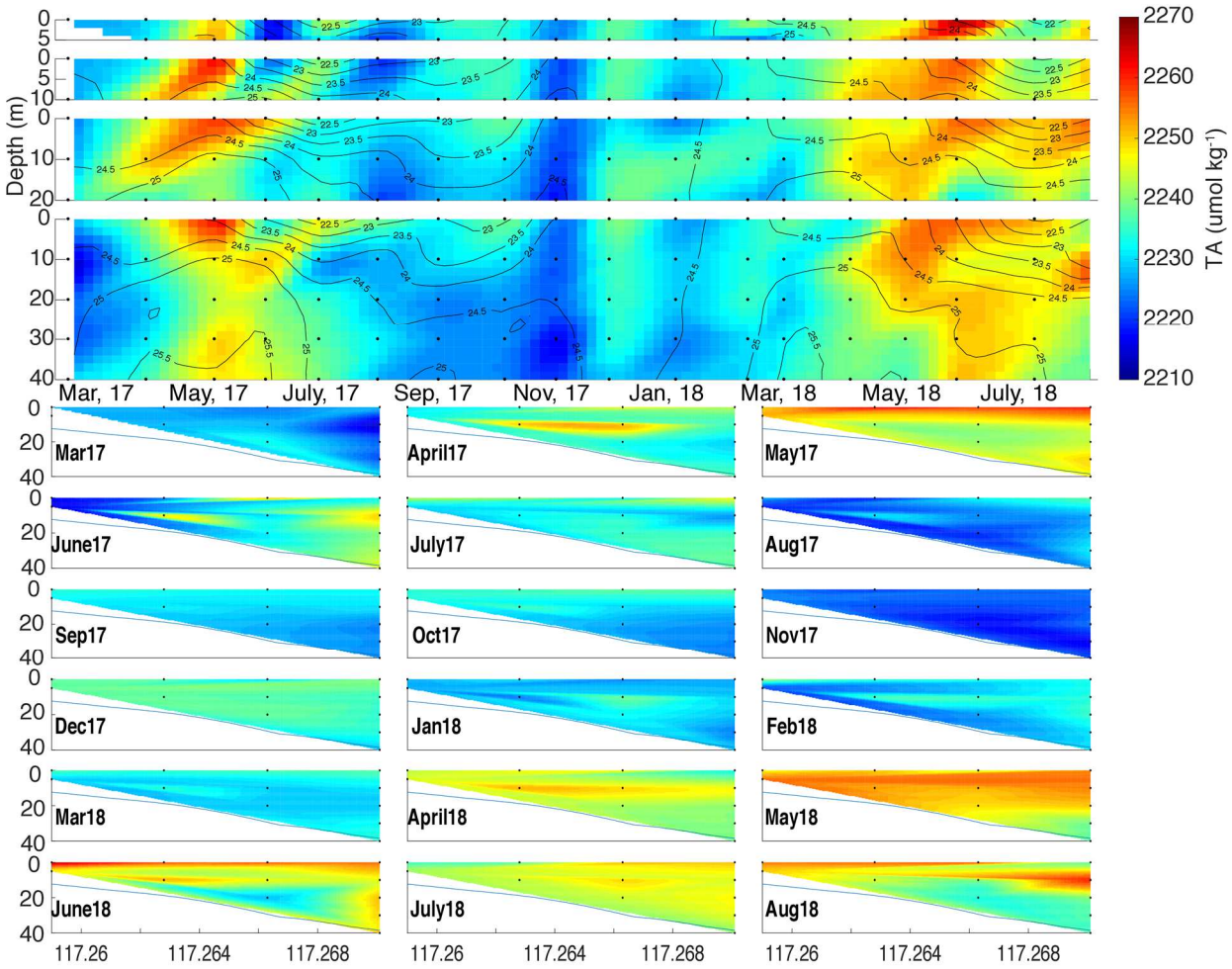

Figure 9. Spatial contour plots from gridded interpolations (cubic interpolations using MATLAB griddata) of TA through time at each station and across each transect. The top most plot of the four plots is the most near-shore station while the lowest plot is the most offshore station. The black contour lines represent calculated isopycnals and the black dots indicate depth of discrete samples. The blue line depicts interpolated bottom depth.

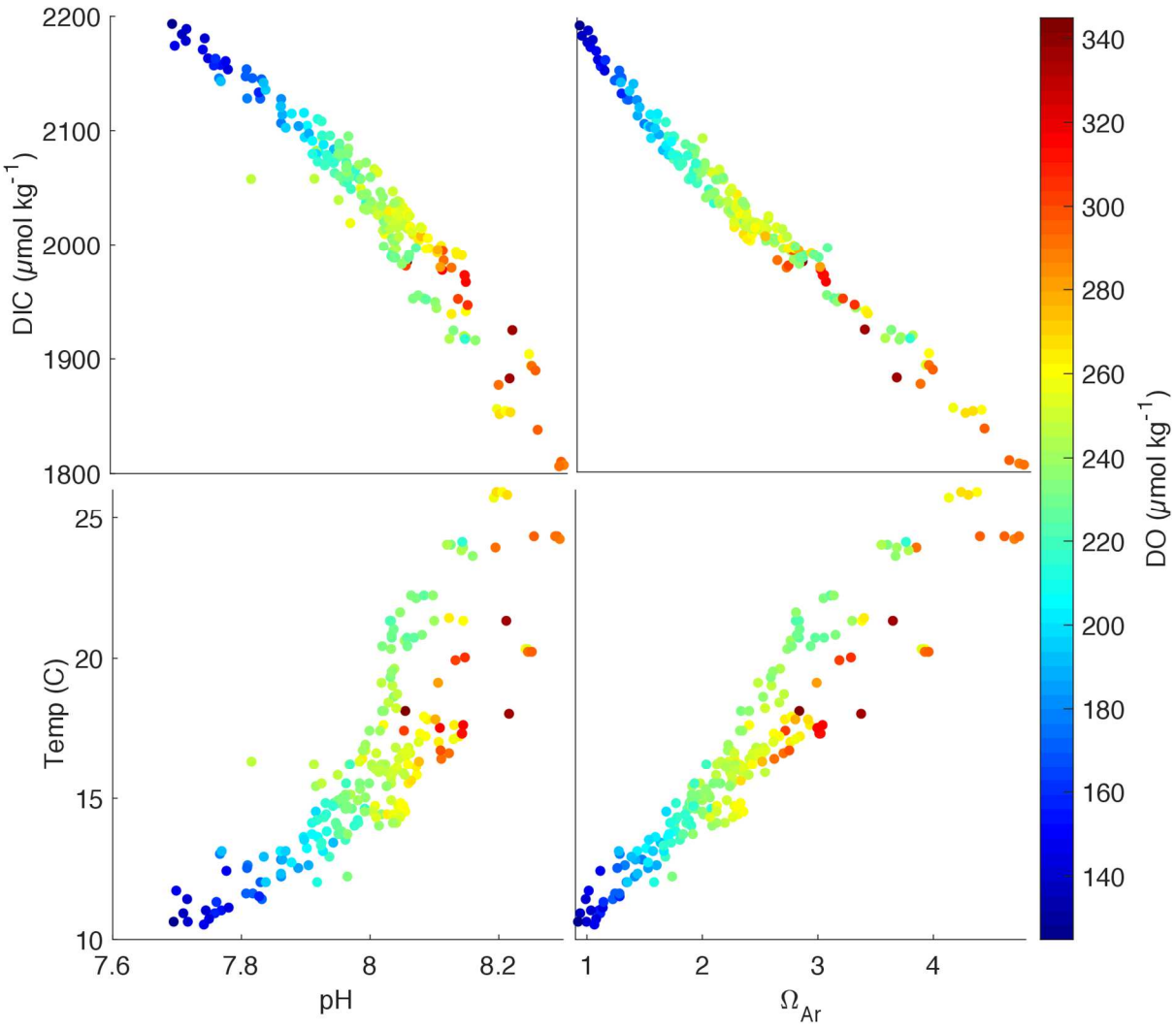

Figure 10. Property-property plots of biogeochemical parameters calculated or measured from discrete seawater bottle samples throughout the study.

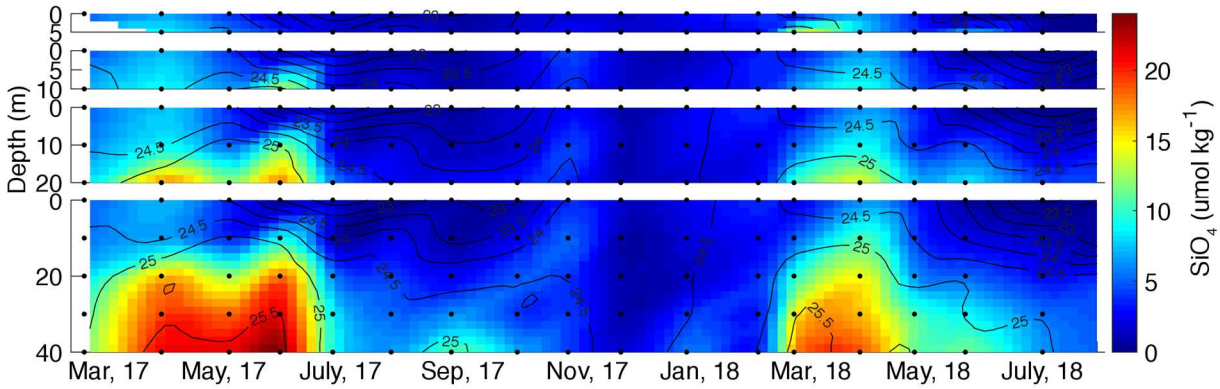

Figure 11. Spatial contour plots from gridded interpolations (cubic interpolations using MATLAB griddata) of [SiO_4] through time at each station and across each transect. The top most plot of the four plots is the most near-shore station while the lowest plot is the most offshore station. The black contour lines represent calculated isopycnals and the black dots indicate depth of discrete samples.

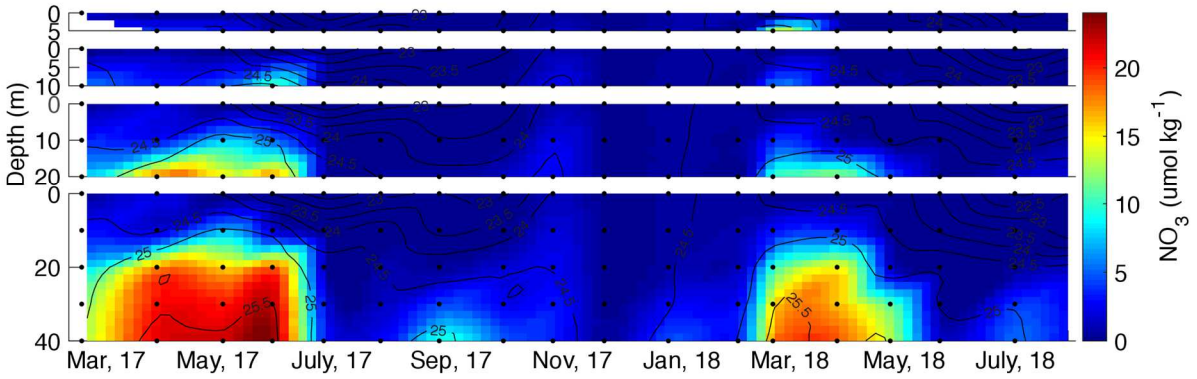

Figure 12. Spatial contour plots from gridded interpolations (cubic interpolations using MATLAB griddata) of [NO_3] through time at each station and across each transect. The top most plot of the four plots is the most near-shore station while the lowest plot is the most offshore station. The black contour lines represent calculated isopycnals and the black dots indicate depth of discrete samples.

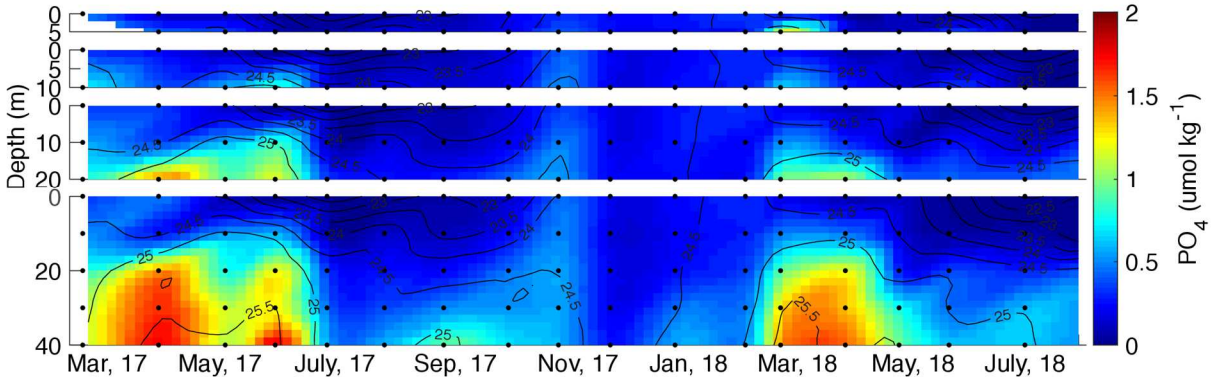

Figure 13. Spatial contour plots from gridded interpolations (cubic interpolations using MATLAB griddata) of [PO_4] through time at each station and across each transect. The top most plot of the four plots is the most near-shore station while the lowest plot is the most offshore station. The black contour lines represent calculated isopycnals and the black dots indicate depth of discrete samples.

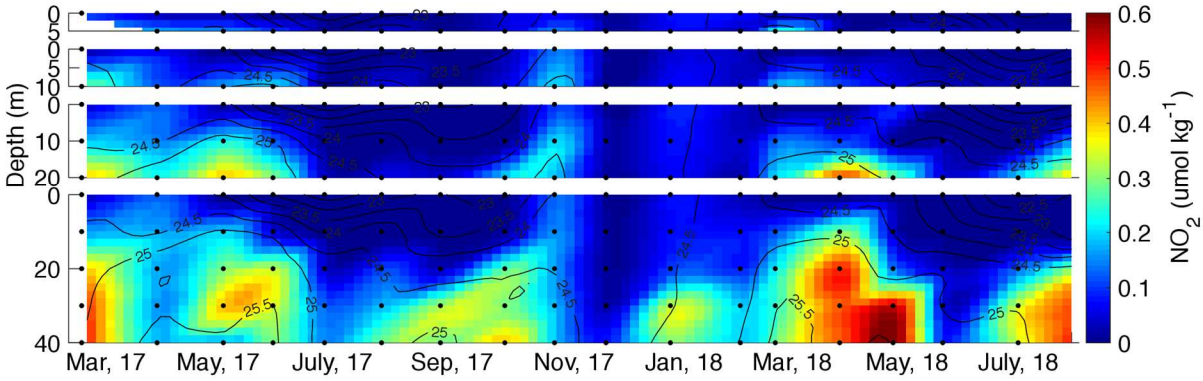

Figure 14. Spatial contour plots from gridded interpolations (cubic interpolations using MATLAB griddata) of [NO_2] through time at each station and across each transect. The top most plot of the four plots is the most near-shore station while the lowest plot is the most offshore station. The black contour lines represent calculated isopycnals and the black dots indicate depth of discrete samples.

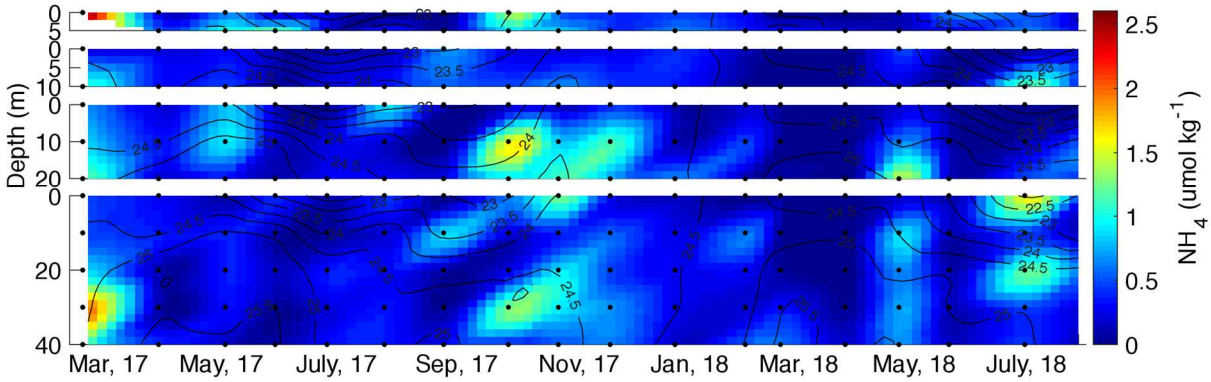

Figure 15. Spatial contour plots from gridded interpolations (cubic interpolations using MATLAB griddata) of [NH_4] through time at each station and across each transect. The top most plot of the four plots is the most near-shore station while the lowest plot is the most offshore station. The black contour lines represent calculated isopycnals and the black dots indicate depth of discrete samples.

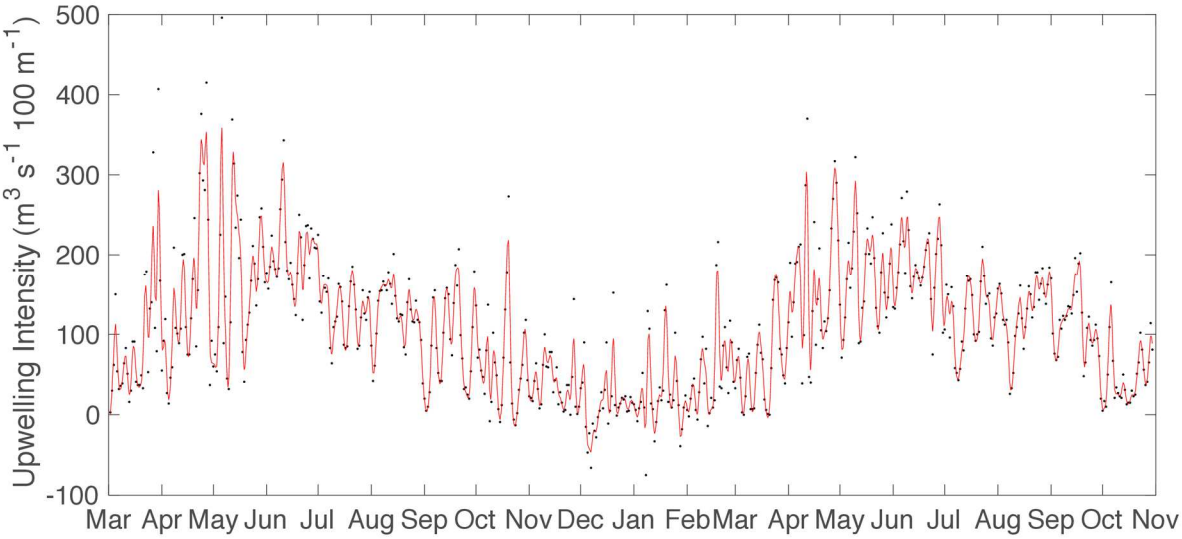

Figure 16. Time series of upwelling intensity from PFEL from March, 2017 to November, 2018. Black dots signify data points while the red line is the spline filtered data (p = 0.8805).

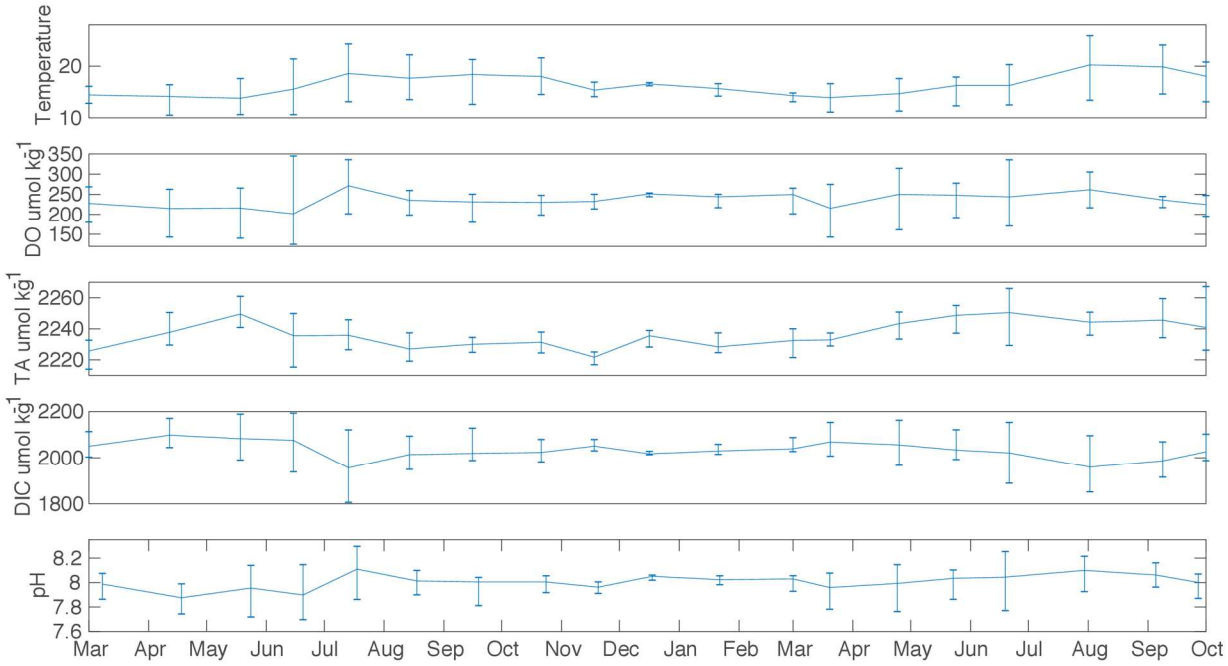

Figure 17. Plotted average and range of temperature, DO, TA, DIC, and pH from discrete seawater samples through March, 2017 to October, 2018.

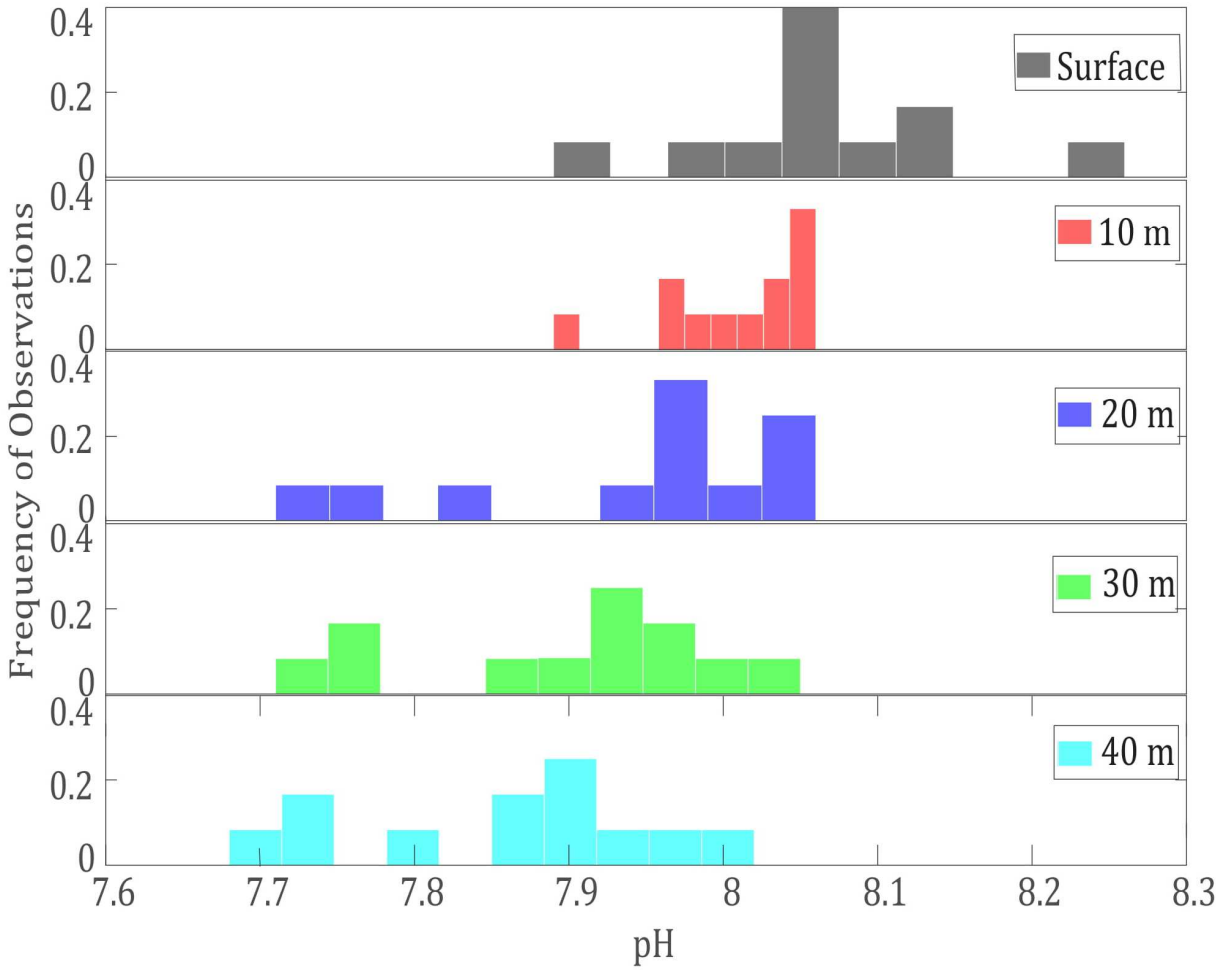

Figure 18. Histogram of pH from discrete seawater samples illustrating pH exposure intensity and duration at 10 m depth bins.

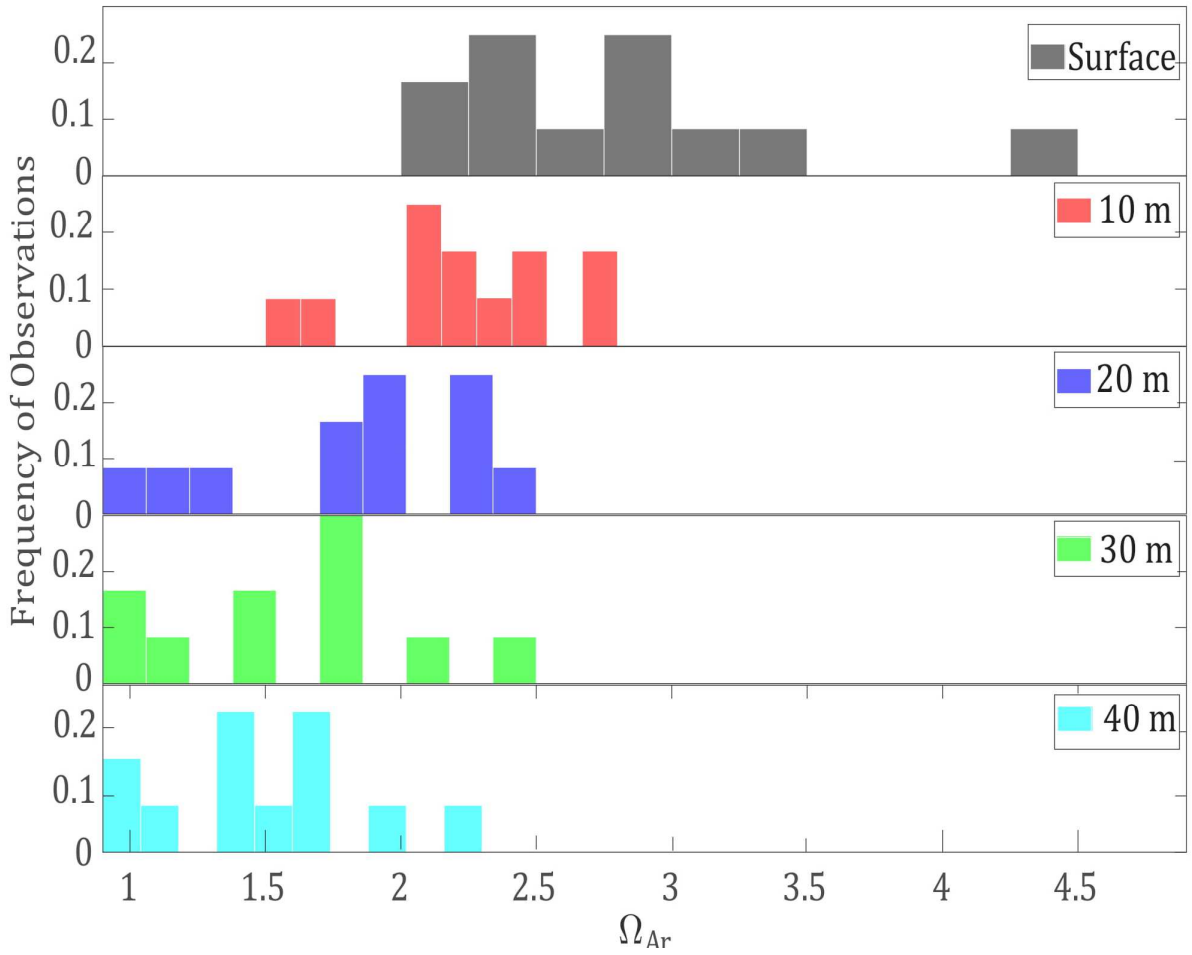

Figure 19. Histogram of Ω_{Ar} from discrete seawater samples illustrating pH exposure intensity and duration at 10 m depth bins.

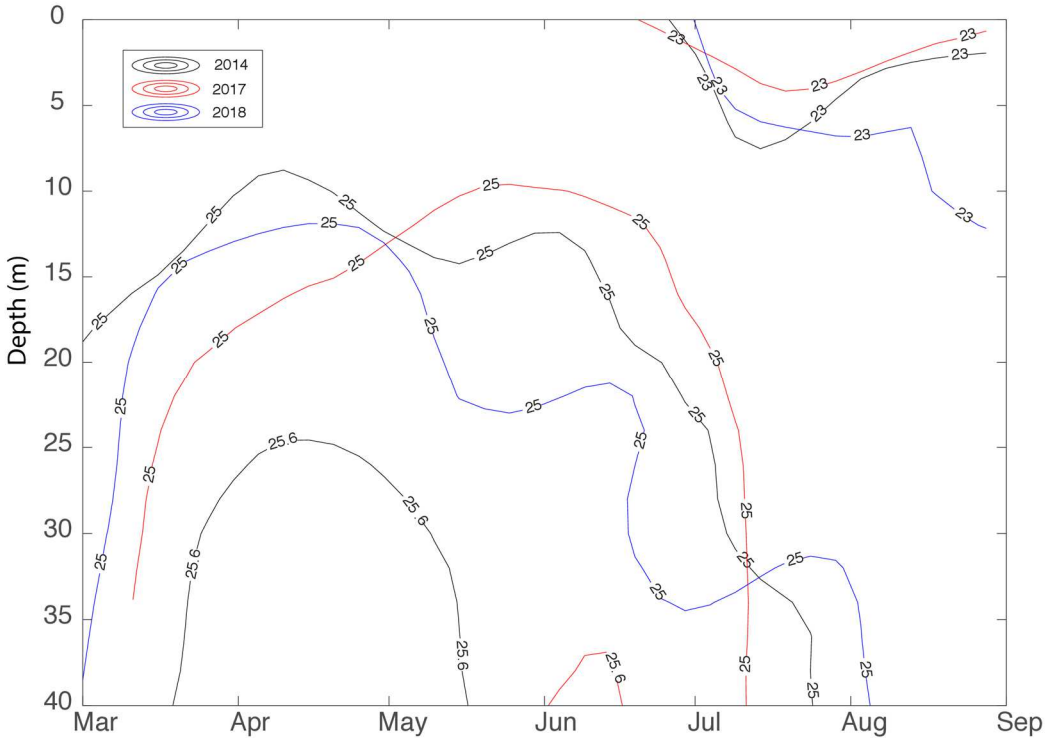

Figure 20. 23.0, 25.0, and 25.6 kg m^{-3} isopycnals (calculated from MATLAB, GSW toolbox) from March to September of 2014 (black), 2017 (red), and 2018 (blue).

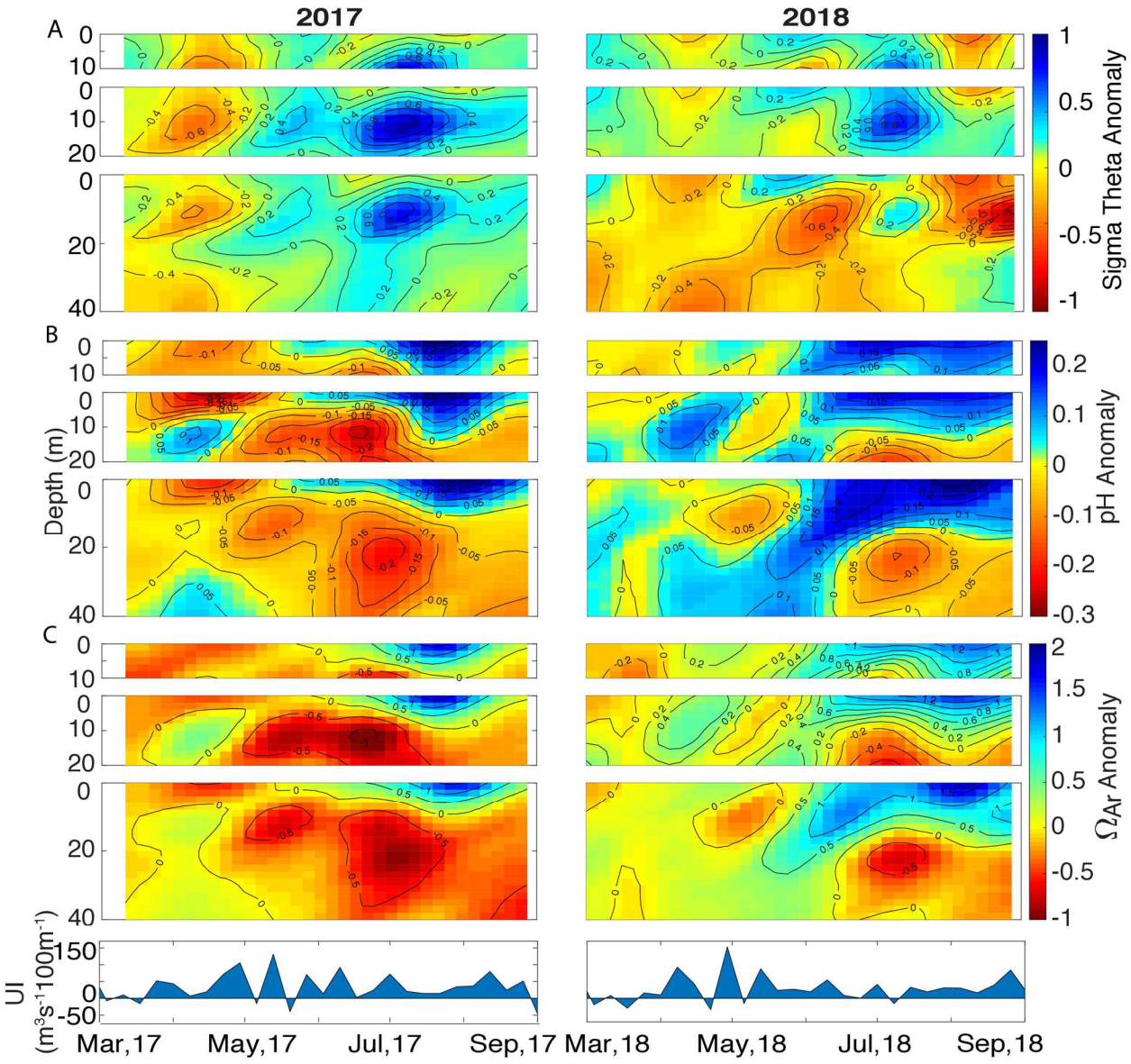

Figure 21. Seasonal variability of (A) density, (B) pH, and (C) Ω_{Ar} between different years from March to August in relation to upwelling intensity.

Table 1: Average daily mean (±SD) and average daily range (±SD) of temperature, salinity, DO and pH from the SeapHOx at ~18m depth during this study.

	Average Daily Mean		Average Daily Range	
	Apr - Aug (n=110)	Aug - Nov (n=95)	Apr - Aug (n=110)	Aug - Nov (n=95)
Temperature	13.5±1.6	16.4±0.8	4.1±1.6	4.7±1.6
Salinity	33.4±0.2	33.4±0.1	0.3±0.2	0.2±0.1
DO (μmol kg^{-1})	150±24	222±14	80±31	32±15
pH	7.85±0.07	8.00±0.02	0.10±0.04	0.09±0.04

Table 2: The average (±SD) and range (±SD) of different seawater carbon chemistry parameters measured during throughout the survey, separated by upwelling season March-August and non-upwelling season September-February.

		March-August, 2017	September, 2017 - February, 2018	March-August, 2018
Average	T	15.9±3.6	16.4±1.3	17.4±3.4
	DO	228±43	240±13	242±36
	DIC	2046±75	2030±22	2024±77
	TA	2233±11	2230±4	2244±6
	pH	7.97±0.13	8.02±0.04	8.03±0.12
	Ar	2.18±0.77	2.29±0.25	2.53±0.81
Range	T	8.7±2.8	3.9±3.2	8.3±2.7
	DO	125±53	44±22	109±51
	DIC	191±76	67±44	189±56
	TA	39±22	14±4	20±10
	pH	0.33±0.11	0.12±0.06	0.31±0.10
	Ar	1.92±0.80	0.79±0.45	2.07±0.69

References

Alin, S. R., Feely, R. A., Dickson, A. G., Martín Hernández-Ayón, J., Juranek, L. W., Ohman, M. D., & Goericke, R. (2012). Robust empirical relationships for estimating the carbonate system in the southern California Current System and application to CalCOFI hydrographic cruise data (2005-2011). *Journal of Geophysical Research: Oceans*, *117*(5). https://doi.org/10.1029/2011JC007511

Andersson, A. J., & MacKenzie, F. T. (2012). Revisiting four scientific debates in ocean acidification research. *Biogeosciences*, *9*(3), 893–905. https://doi.org/10.5194/bg-9-893-2012

Andersson, A.J., Kline, D.I., Edmunds, P.J., Archer, S.D., Bednaršek, N., Carpenter, R.C., Chadsey, M., Goldstein, P., Grottoli, A.G., Hurst, T.P. and King, A.L., 2015. Understanding ocean acidification impacts on organismal to ecological scales. *Oceanography*, *28*(2), pp.16-27. https://doi.org/10.5670/oceanog.2015.27

Andersson, Andreas J., & Gledhill, D. (2013). Ocean Acidification and Coral Reefs: Effects on Breakdown, Dissolution, and Net Ecosystem Calcification. *Annual Review of Marine Science*, *5*(1), 321–348. https://doi.org/10.1146/annurev-marine-121211-172241

Andersson, Andreas J., Yeakel, K. L., Bates, N. R., & De Putron, S. J. (2014). Partial offsets in ocean acidification from changing coral reef biogeochemistry. *Nature Climate Change*. https://doi.org/10.1038/nclimate2050

Armstrong, F. A. J., Stearns, C. R., & Strickland, J. D. H. (1967). The measurement of upwelling and subsequent biological process by means of the Technicon Autoanalyzer® and associated equipment. *Deep Sea Research and Oceanographic Abstracts*, *14*(3), 381–389. https://doi.org/10.1016/0011-7471(67)90082-4

Bakun, A. (1973). Coastal upwelling indices, west coast of North America, 1946-71.

Bakun, A. (1975). Daily and weekly upwelling indices, west coast of North America, 1967-73.

Bakun, A., Black, B. A., Bograd, S. J., García-Reyes, M., Miller, A. J., Rykaczewski, R. R., & Sydeman, W. J. (2015, June 1). Anticipated Effects of Climate Change on Coastal Upwelling Ecosystems. *Current Climate Change Reports*, Vol. 1, pp. 85–93. https://doi.org/10.1007/s40641-015-0008-4

Barton, A., Hales, B., Waldbusser, G. G., Langdon, C., & Feelyd, R. A. (2012). The Pacific oyster, Crassostrea gigas, shows negative correlation to naturally elevated carbon dioxide levels: Implications for near-term ocean acidification effects. *Limnology and Oceanography*, *57*(3), 698–710. https://doi.org/10.4319/lo.2012.57.3.0698

Bates, N. R., & Peters, A. J. (2007). The contribution of atmospheric acid deposition to ocean acidification in the subtropical North Atlantic Ocean. *Marine Chemistry*, *107*(4), 547-558. https://doi.org/10.1016/j.marchem.2007.08.002

Bates, N.R., Astor, Y.M., Church, M.J., Currie, K., Dore, J.E., González-Dávila, M., Lorenzoni,

L., Muller-Karger, F., Olafsson, J. and Santana-Casiano, J.M., 2014. A Time-Series View of Changing Surface Ocean Chemistry Due to Ocean Uptake of Anthropogenic CO□ and Ocean Acidification. *Oceanography*, *27*(1), pp.126-141. https://doi.org/10.5670/oceanog.2014.16

Bates, N. R., Amat, A., & Andersson, A. J. (2010). Feedbacks and responses of coral calcification on the Bermuda reef system to seasonal changes in biological processes and ocean acidification. *Biogeosciences*, *7*(8), 2509–2530. https://doi.org/10.5194/bg-7-2509-2010

Bates, N. R., Best, M. H. P., Neely, K., Garley, R., Dickson, A. G., & Johnson, R. J. (2012). Detecting anthropogenic carbon dioxide uptake and ocean acidification in the North Atlantic Ocean. *Biogeosciences*, *9*(7), 2509–2522. https://doi.org/10.5194/bg-9-2509-2012

Bednaršek, N., Feely, R. A., Reum, J. C. P., Peterson, B., Menkel, J., Alin, S. R., & Hales, B. (2014). Limacina helicina shell dissolution as an indicator of declining habitat suitability owing to ocean acidification in the California Current Ecosystem. *Proceedings of the Royal Society B: Biological Sciences*, *281*(1785). https://doi.org/10.1098/rspb.2014.0123

Bernhardt, H., & Wilhelms, A. (1967, October). The continuous determination of low level iron, soluble phosphate and total phosphate with the AutoAnalyzer. In *Technicon Symposia* (Vol. 1, pp. 385-389).

Bograd, S. J., Schroeder, I., Sarkar, N., Qiu, X., Sydeman, W. J., & Schwing, F. B. (2009). Phenology of coastal upwelling in the California Current. *Geophysical Research Letters*. https://doi.org/10.1029/2008GL035933

Booth, J.A.T., McPhee-Shaw, E.E., Chua, P., Kingsley, E., Denny, M., Phillips, R., Bograd, S.J., Zeidberg, L.D. and Gilly, W.F., 2012. Natural intrusions of hypoxic, low pH water into nearshore marine environments on the California coast. *Continental Shelf Research*, *45*, 108-115. https://doi.org/10.1016/j.csr.2012.06.009

Borges, A. V., Delille, B., & Frankignoulle, M. (2005). Budgeting sinks and sources of CO2 in the coastal ocean: Diversity of ecosystem counts. *Geophysical Research Letters*, *32*(14), 1–4. https://doi.org/10.1029/2005GL023053

Brady, R. X., Lovenduski, N. S., Alexander, M. A., Jacox, M., & Gruber, N. (2019). On the role of climate modes in modulating the air-sea CO 2 fluxes in eastern boundary upwelling systems. *Biogeosciences*, *16*(2), 329–346. https://doi.org/10.5194/bg-16-329-2019

Bresnahan, P. J., Martz, T. R., Takeshita, Y., Johnson, K. S., & LaShomb, M. (2014). Best practices for autonomous measurement of seawater pH with the Honeywell Durafet. *Methods in Oceanography*. https://doi.org/10.1016/j.mio.2014.08.003

Bylhouwer, B., Ianson, D., & Kohfeld, K. (2013). Changes in the onset and intensity of wind-driven upwelling and downwelling along the North American Pacific coast. *Journal of Geophysical Research: Oceans*, *118*(5), 2565–2580. https://doi.org/10.1002/jgrc.20194

Cai, W.J., Hu, X., Huang, W.J., Murrell, M.C., Lehrter, J.C., Lohrenz, S.E., Chou, W.C., Zhai, W., Hollibaugh, J.T., Wang, Y. and Zhao, P., 2011. Acidification of subsurface coastal waters enhanced by eutrophication. *Nature geoscience*, *4*(11), 766–770.

https://doi.org/10.1038/ngeo1297

Caldeira, K., & Wickett, M. E. (2003). Oceanography: anthropogenic carbon and ocean pH. *Nature*, *425*(6956), 365.

C. D. Keeling, S. C. Piper, R. B. Bacastow, M. Wahlen, T. P. Whorf, M. Heimann, and H. A. Meijer, Exchanges of atmospheric CO2 and 13CO2 with the terrestrial biosphere and oceans from 1978 to 2000. I. Global aspects, SIO Reference Series, No. 01-06, Scripps Institution of Oceanography, San Diego, 88 pages, 2001. http://escholarship.org/uc/item/09v319r9

Ciais, P., Gasser, T., Paris, J.D., Caldeira, K., Raupach, M.R., Canadell, J.G., Patwardhan, A., Friedlingstein, P., Piao, S.L. and Gitz, V., 2013. Attributing the increase in atmospheric CO 2 to emitters and absorbers. *Nature Climate Change*, *3*(10), 926–930. https://doi.org/10.1038/nclimate1942

Cyronak, T., Andersson, A.J., D'Angelo, S., Bresnahan, P., Davidson, C., Griffin, A., Kindeberg, T., Pennise, J., Takeshita, Y. and White, M., 2018. Short-term spatial and temporal carbonate chemistry variability in two contrasting seagrass meadows: implications for pH buffering capacities. *Estuaries and Coasts*, *41*(5), pp.1282-1296. https://doi.org/10.1007/s12237-017-0356-5

Cyronak, T., Schulz, K. G., Santos, I. R., & Eyre, B. D. (2014). Enhanced acidification of global coral reefs driven by regional biogeochemical feedbacks. *Geophysical Research Letters*. https://doi.org/10.1002/2014GL060849

Davidson, C.: Spatial and Temporal Variability of Coastal Carbonate Chemistry in the Southern California Region, M.S. thesis, University of California San Diego. Ann Arbor, USA, ProQuest Dissertations and Theses (Publication no. 1591920), 2015

Davis, N., & VanBlaricom, G. R. (1978). Spatial and temporal heterogeneity in a sand bottom epifaunal community of invertebrates in shallow water 1. *Limnology and Oceanography*, *23*(3), 417-427.

Di Lorenzo, E. (2003). Seasonal dynamics of the surface circulation in the Southern California Current System. *Deep Sea Research Part II: Topical Studies in Oceanography*, *50*(14-16), 2371-2388.

Di Lorenzo, E. (2015). Climate science: The future of coastal ocean upwelling. *Nature*, *518*(7539). https://doi.org/10.1038/518310a

Dickson, A. G. (Andrew G., Sabine, C. L., Christian, J. R., & North Pacific Marine Science Organization. (2007). *Guide to best practices for ocean CO measurements*. North Pacific Marine Science Organization.

Dickson, A. G., & Millero~, F. J. (1987). A comparison of the equilibrium constants for the dissociation of carbonic acid in seawater media. In *Deep-Sea Research* (Vol. 34).

Duarte, C.M., Hendriks, I.E., Moore, T.S., Olsen, Y.S., Steckbauer, A., Ramajo, L., Carstensen, J., Trotter, J.A. and McCulloch, M., 2013. Is ocean acidification an open-ocean syndrome? Understanding anthropogenic impacts on seawater pH. *Estuaries and Coasts*, *36*(2), 221–

236. https://doi.org/10.1007/s12237-013-9594-3

Fassbender, A. J., Sabine, C. L., Feely, R. A., Langdon, C., & Mordy, C. W. (2011). Inorganic carbon dynamics during northern California coastal upwelling. *Continental Shelf Research*, *31*(11). https://doi.org/10.1016/j.csr.2011.04.006

Feely, R.A., Alin, S.R., Carter, B., Bednaršek, N., Hales, B., Chan, F., Hill, T.M., Gaylord, B., Sanford, E., Byrne, R.H. and Sabine, C.L., 2016. Chemical and biological impacts of ocean acidification along the west coast of North America. *Estuarine, Coastal and Shelf Science*, *183*, 260-270. https://doi.org/10.1016/j.ecss.2016.08.043

Feely, R. A., Sabine, C. L., Lee, K., Berelson, W., Kleypas, J., Fabry, V. J., & Millero, F. J. (2013). *Impact of Anthropogenic CO 2 on the CaCO 3 System in the Oceans*. Retrieved from http://science.sciencemag.org/

Feely, R. A., Doney, S. C., & Cooley, S. R. (2009). Ocean acidification: Present conditions and future changes in a high-CO□ world. *Oceanography*, *22*(4), 36-47.

Feely, R. A., Sabine, C. L., Hernandez-Ayon, J. M., Ianson, D., & Hales, B. (2008). Evidence for upwelling of corrosive "acidified" water onto the continental shelf. *Science*. https://doi.org/10.1126/science.1155676

Fenberg, P. B., Menge, B. A., Raimondi, P. T., & Rivadeneira, M. M. (2015). Biogeographic structure of the northeastern Pacific rocky intertidal: The role of upwelling and dispersal to drive patterns. *Ecography*, *38*(1), 83–95. https://doi.org/10.1111/ecog.00880

Frieder, C. A., Nam, S. H., Martz, T. R., & Levin, L. A. (2012). High temporal and spatial variability of dissolved oxygen and pH in a nearshore California kelp forest. *Biogeosciences*, *9*(10), 3917–3930. https://doi.org/10.5194/bg-9-3917-2012

Frieder, Christina A., Gonzalez, J. P., Bockmon, E. E., Navarro, M. O., & Levin, L. A. (2014). Can variable pH and low oxygen moderate ocean acidification outcomes for mussel larvae? *Global Change Biology*, *20*(3), 754–764. https://doi.org/10.1111/gcb.12485

Friedlingstein, P., Houghton, R.A., Marland, G., Hackler, J., Boden, T.A., Conway, T.J., Canadell, J.G., Raupach, M.R., Ciais, P. and Le Quéré, C., 2010. Update on CO2 emissions. *Nature Geoscience*, Vol. 3, pp. 811–812. https://doi.org/10.1038/ngeo1022

Friedrich, T., Timmermann, A., Abe-Ouchi, A., Bates, N.R., Chikamoto, M.O., Church, M.J., Dore, J.E., Gledhill, D.K., Gonzalez-Davila, M., Heinemann, M. and Ilyina, T., 2012. Detecting regional anthropogenic trends in ocean acidification against natural variability. *Nature Climate Change*, *2*(3), 167–171. https://doi.org/10.1038/nclimate1372

Gaylord, B., Hill, T.M., Sanford, E., Lenz, E.A., Jacobs, L.A., Sato, K.N., Russell, A.D. and Hettinger, A., 2011. Functional impacts of ocean acidification in an ecologically critical foundation species. *Journal of Experimental Biology*, *214*(15), 2586–2594. https://doi.org/10.1242/jeb.055939

Gruber, N., Hauri, C., Lachkar, Z., Loher, D., Frolicher, T. L., & Plattner, G.-K. (2012). Rapid Progression of Ocean Acidification in the California Current System. *Science*. https://doi.org/10.1126/science.1216773

Hales, B., Karp-Boss, L., Perlin, A., & Wheeler, P. A. (2006). Oxygen production and carbon sequestration in an upwelling coastal margin. *Global Biogeochemical Cycles*, *20*(3). https://doi.org/10.1029/2005GB002517

Hare, C.E., Leblanc, K., DiTullio, G.R., Kudela, R.M., Zhang, Y., Lee, P.A., Riseman, S. and Hutchins, D.A., 2007. Consequences of increased temperature and CO2 for phytoplankton community structure in the Bering Sea. *Marine Ecology Progress Series*, *352*, 9–16. https://doi.org/10.3354/meps07182

Harris, K. E., DeGrandpre, M. D., & Hales, B. (2013). Aragonite saturation state dynamics in a coastal upwelling zone. *Geophysical Research Letters*, *40*(11), 2720–2725. https://doi.org/10.1002/grl.50460

Hauri, C., Gruber, N., Vogt, M., Doney, S.C., Feely, R.A., Lachkar, Z., Leinweber, A., McDonnell, A.M., Münnich, M. and Plattner, G.K., 2013. Spatiotemporal variability and long-term trends of ocean acidification in the California Current System. *Biogeosciences*, *10*(1), 193-216. https://doi.org/10.5194/bg-10-193-2013

Hauri, Claudine, Gruber, N., Plattner, G.-K., Alin, S., Feely, R., Hales, B., & Wheeler, P. (2009). OCEAN ACIDIFICATION IN THE CALIFORNIA CURRENT SYSTEM. *Oceanography*. https://doi.org/10.5670/oceanog.2009.97

Hofmann, G.E., Smith, J.E., Johnson, K.S., Send, U., Levin, L.A., Micheli, F., Paytan, A., Price, N.N., Peterson, B., Takeshita, Y. and Matson, P.G., 2011. High-frequency dynamics of ocean pH: a multi-ecosystem comparison. *PloS one*, *6*(12). https://doi.org/10.1371/journal.pone.0028983

Hydes, D., Aoyama, M., Aminot, A., Bakker, K., Becker, S., Coverly, S., Daniel, A., Dickson, A., Grosso, O., Kerouel, R. and Van Ooijen, J., 2010. Determination of dissolved nutrients (N, P, Si) in seawater with high precision and inter-comparability using gas-segmented continuous flow analysers.

Iles, A. C., Gouhier, T. C., Menge, B. A., Stewart, J. S., Haupt, A. J., & Lynch, M. C. (2012). Climate-driven trends and ecological implications of event-scale upwelling in the California Current System. *Global Change Biology*. https://doi.org/10.1111/j.1365-2486.2011.02567.x

IPCC, 2014: *Climate Change 2014: Synthesis Report. Contribution of Working Groups I, II and III to the Fifth Assessment Report of the Intergovernmental Panel on Climate Change* [Core Writing Team, R.K. Pachauri and L.A. Meyer (eds.)]. IPCC, Geneva, Switzerland, 151 pp.

Jansen, E. ; Overpeck, J. ; Briffa, K. R. ; Duplessy, J. C. & Joos, F. (2007). Masson-Delmotte, V. 2007."Palaeoclimate". In S. Solomon, D. Qin, M. Manning, Z. Chen, M. Marquis, K. B. Averyt, M. Tignor & H. L. Miller (eds.), *Climate Change 2007: The Physical Science Basis. Contribution of Working Group I to the Fourth Assessment Report of the Intergovernmental Panel on Climate Change*. Cambridge University Press.

Kapsenberg, L., & Hofmann, G. E. (2016). Ocean pH time-series and drivers of variability along the northern Channel Islands, California, USA. *Limnology and Oceanography*, *61*(3), 953–968. https://doi.org/10.1002/lno.10264

Koch, M., Bowes, G., Ross, C., & Zhang, X. H. (2013). Climate change and ocean acidification effects on seagrasses and marine macroalgae. *Global change biology*, *19*(1), 103-132.

Kroeker, K. J., Micheli, F., Gambi, M. C., & Martz, T. R. (2011). Divergent ecosystem responses within a benthic marine community to ocean acidification. *Proceedings of the National Academy of Sciences of the United States of America*, *108*(35), 14515–14520. https://doi.org/10.1073/pnas.1107789108

Largier, J. L., Hollibaugh, J. T., & Smith, S. V. (1997). Seasonally hypersaline estuaries in Mediterranean-climate regions. *Estuarine, Coastal and Shelf Science*. https://doi.org/10.1006/ecss.1997.0279

Laruelle, G. G., Dürr, H. H., Slomp, C. P., & Borges, A. V. (2010). Evaluation of sinks and sources of CO2 in the global coastal ocean using a spatially-explicit typology of estuaries and continental shelves. *Geophysical Research Letters*, *37*(15). https://doi.org/10.1029/2010GL043691

Laruelle, G. G., Lauerwald, R., Pfeil, B., & Regnier, P. (2014). Regionalized global budget of the CO2 exchange at the air-water interface in continental shelf seas. *Global Biogeochemical Cycles*, *28*(11), 1199–1214. https://doi.org/10.1002/2014GB004832

Lauvset, S. K., Gruber, N., Landschützer, P., Olsen, A., & Tjiputra, J. (2015). Trends and drivers in global surface ocean pH over the past 3 decades. *Biogeosciences*. https://doi.org/10.5194/bg-12-1285-2015

Leinweber, A., & Gruber, N. (2013). Variability and trends of ocean acidification in the Southern California Current System: A time series from Santa Monica Bay. *Journal of Geophysical Research: Oceans*, *118*(7), 3622–3633. https://doi.org/10.1002/jgrc.20259

Lucas, A. J., Franks, P. J., & Dupont, C. L. (2011). Horizontal internal□tide fluxes support elevated phytoplankton productivity over the inner continental shelf. *Limnology and Oceanography: Fluids and Environments*, *1*(1), 56-74.

Martz, T. R., Connery, J. G., & Johnson, K. S. (2010). Testing the Honeywell Durafet® for seawater pH applications. *Limnology and Oceanography: Methods*. https://doi.org/10.4319/lom.2010.8.172

McDougall, T. J., and Barker, P. M. (2011). *Getting Started with TEOS-10 and the Gibbs Seawater (GSW) Oceanographic Toolbox.* Sydney: SCOR/IAPSO WG 127, 1–28.

Mehrbach, C., Culberson, C. H., Hawley, J. E., & Pytkowicx, R. M. (n.d.). *MEASUREMENT OF THE APPARENT DISSOCIATION CONSTANTS OF CARBONIC ACID IN SEAWATER AT ATMOSPHERIC PRESSURE1*.

Morin, J. G., Kastendiek, J. E., Harrington, A., & Davis, N. (1985). Organization and patterns of interactions in a subtidal sand community on an exposed coast. *Marine Ecology Progress Series*, *27*, 163-185.

Navarro, M. O., Parnell, P. E., and Levin, L. A.: Year-round spawning of the Market Squid,

Doryteuthis opalescens and associated critical habitat along an upwelling margin, in: Coastal and Estuarine Research Federation National Conference, San Diego, 2013.

Olafsson, J., Olafsdottir, S. R., Benoit-Cattin, A., Danielsen, M., Arnarson, T. S., & Takahashi, T. (2009). Rate of Iceland Sea acidification from time series measurements. *Biogeosciences*, *6*(11). https://doi.org/10.5194/bgd-6-5251-2009

Orr, J.C., Fabry, V.J., Aumont, O., Bopp, L., Doney, S.C., Feely, R.A., Gnanadesikan, A., Gruber, N., Ishida, A., Joos, F. and Key, R.M., 2005. Anthropogenic ocean acidification over the twenty-first century and its impact on calcifying organisms. *Nature*, *437*(7059), 681-686. https://doi.org/10.1038/nature04095

Paull, C.K., Caress, D.W., Lundsten, E., Gwiazda, R., Anderson, K., McGann, M., Conrad, J., Edwards, B. and Sumner, E.J., 2013. Anatomy of the La Jolla submarine canyon system; offshore Southern California. *Marine Geology*, *335*, 16–34. https://doi.org/10.1016/j.margeo.2012.10.003

Pauly, D., & Christensen, V. (1995). Primary production required to sustain global fisheries. *Nature*, *374*(6519), 255.Pavía, E. G., & Badan, A. (1998). ENSO modulates rainfall in the Mediterranean Californias. *Geophysical Research Letters*, *25*(20), 3855–3858. https://doi.org/10.1029/1998GL900029

Pavia, E. G., & Graef, F. (2002). The recent rainfall climatology of the Mediterranean Californias. *Journal of Climate*, *15*(18), 2697-2701.

Quéré, C., Andrew, R.M., Friedlingstein, P., Sitch, S., Hauck, J., Pongratz, J., Pickers, P.A., Korsbakken, J.I., Peters, G.P., Canadell, J.G. and Arneth, A., 2018. Global carbon budget 2018. *Earth System Science Data*, *10*(4), 2141–2194. https://doi.org/10.5194/essd-10-2141-2018

Revelle, R., & Suess, H. E. (1957). Carbon dioxide exchange between atmosphere and ocean and the question of an increase of atmospheric CO2 during the past decades. *Tellus*, *9*(1), 18-27.

Sabine, C.L., Feely, R.A., Gruber, N., Key, R.M., Lee, K., Bullister, J.L., Wanninkhof, R., Wong, C.S.L., Wallace, D.W., Tilbrook, B. and Millero, F.J., 2004. The oceanic sink for anthropogenic CO2. *science*, *305*(5682), pp.367-371. Retrieved from http://science.sciencemag.org/

Silbiger, N. J., & Sorte, C. J. B. (2018). Biophysical feedbacks mediate carbonate chemistry in coastal ecosystems across spatiotemporal gradients. *Scientific Reports*, *8*(1). https://doi.org/10.1038/s41598-017-18736-6

Snyder, M. A., Sloan, L. C., Diffenbaugh, N. S., & Bell, J. L. (2003). Future climate change and upwelling in the California Current. *Geophysical Research Letters*. https://doi.org/10.1029/2003GL017647

Sutton, A.J., Feely, R.A., Maenner-Jones, S., Musielwicz, S., Osborne, J., Dietrich, C., Monacci, N., Cross, J., Bott, R., Kozyr, A. and Andersson, A.J., 2019. Autonomous seawater pCO 2 and pH time series from 40 surface buoys and the emergence of anthropogenic trends. *Earth System Science Data*, *11*(1), 421–439. https://doi.org/10.5194/essd-11-421-2019

Swart, N. C., Allen, S. E., & Greenan, B. J. W. (2011). Resonant amplification of subinertial tides in a submarine canyon. *Journal of Geophysical Research: Oceans*, *116*(9). https://doi.org/10.1029/2011JC006990

Sydeman, W. J., Garcia-Reyes, M., Schoeman, D. S., Rykaczewski, R. R., Thompson, S. A., Black, B. A., & Bograd, S. J. (2014). Climate change and wind intensification in coastal upwelling ecosystems. *Science*, *345*(6192). https://doi.org/10.1126/science.1251635

Takeshita, Y., Frieder, C.A., Martz, T.R., Ballard, J.R., Feely, R.A., Kram, S., Nam, S., Navarro, M.O., Price, N.N. and Smith, J.E., 2015. Including high-frequency variability in coastal ocean acidification projections. *Biogeosciences*. https://doi.org/10.5194/bg-12-5853-2015

Thomsen, J., Gutowska, M., Saphörster, J., Heinemann, A., Trübenbach, K., Fietzke, J., Hiebenthal, C., Eisenhauer, A., Körtzinger, A., Wahl, M. and Melzner, F., 2010. Calcifying invertebrates succeed in a naturally CO2 enriched coastal habitat but are threatened by high levels of future acidification. *Biogeosciences*, *7*(11), pp.3879-3891.https://doi.org/10.5194/bg-7-3879-2010

Thompson, Andrew R., et al. "State of the California Current 2017-2018: Still Not Quite Normal in the North and Gettig Interesting in the South." *CalCOFI Rep.*, vol. 59, no. January 2019, 2018.

Uppström, L. R. (1974). The boron/chlorinity ratio of deep-sea water from the Pacific Ocean. In *Deep Sea Research and Oceanographic Abstracts* (Vol. 21, pp. 161-162).Wang, D., Gouhier, T. C., Menge, B. A., & Ganguly, A. R. (2015). Intensification and spatial homogenization of coastal upwelling under climate change. *Nature*, *518*(7539). https://doi.org/10.1038/nature14235

van Heuven, S., Pierrot, D., Rae, J. W. B., Lewis, E., and Wallace, D. W. R. (2011). *MATLAB Program Developed for CO_2 System Calculations*. *ORNL/CDIAC- 105b*. Oak Ridge: Carbon Dioxide Information Analysis Center, Oak Ridge National Laboratory, U.S. Department of Energy.

Wells, Brian K., et al. "State of the California Current 2016-17: Still Anything But ``Normal'' in the North." *California Cooperative Oceanic Fisheries Investigations Reports*, vol. 58, 2017, pp. 1–55.

Wood, E. D., Armstrong, F. A. J., & Richards, F. A. (1967). Determination of nitrate in sea water by cadmium-copper reduction to nitrite. *Journal of the Marine Biological Association of the United Kingdom*, *47*(1), 23–31. https://doi.org/10.1017/S002531540003352X

Wootton, J. T., Pfister, C. A., & Forester, J. D. (2008). *Dynamic patterns and ecological impacts of declining ocean pH in a high-resolution multi-year dataset*. Retrieved from www.pnas.org/cgi/content/full/

Yu, P. C., Matson, P. G., Martz, T. R., & Hofmann, G. E. (2011). The ocean acidification seascape and its relationship to the performance of calcifying marine invertebrates: Laboratory experiments on the development of urchin larvae framed by environmentally-

relevant pCO2/pH. *Journal of Experimental Marine Biology and Ecology*. https://doi.org/10.1016/j.jembe.2011.02.016